TECHNICAL MEMORANDUM

309

Impact of horizontal resolution on seasonal integrations

Č. Branković and D. Gregory

Research Department

July 2000

European Centre for Medium-Range Weather Forecasts
Europäisches Zentrum für mittelfristige Wettervorhersage
Centre européen pour les prévisions météorologiques à moyen

ABSTRACT

The effects of changing horizontal resolution are studied using ensembles of seasonal simulations made by relatively recent version of the ECMWF model. The model is integrated at T63, T_L159 and T_L319 spectral resolutions. The latter corresponds approximately to a 0.56^O latitude-longitude grid and may be considered, by climate modelling standards, as very high resolution.

Though, on average, no dramatically large differences in ensemble mean quantities are found between the three resolutions, some monotonic (systematic) differences with increasing resolution are evident. Whilst the better representation of orography with increasing resolution accounts for many differences between the resolutions considered, not all variations can be associated with changes in local orographic features. The existence of systematic changes with resolution indicates that the development of numerical models, especially physical parametrizations, should be carried out simultaneously at various resolutions. The study indicates that the highest model resolution does not always give the best results in terms of verification. In addition, reanalysis parameters that are mainly driven by model physics may not be optimal for the verification in such resolution studies.

1. INTRODUCTION

The dependence of atmospheric general circulation models (AGCM) used in climate studies on horizontal resolution is a subject of continuous interest. Despite a constant increase in the computational power, various compromises in model formulation and/or horizontal resolution are normally made for reasons of computational efficiency. The issue of horizontal resolution has become even more important as many centres have adopted a probabilistic approach to seasonal forecasting, i.e. in an operational environment, ensembles of forecasts are made on a (quasi) regular basis. Coupled to ocean models, these multiple long-range AGCM integrations pose a substantial demand on computational resources. Therefore computationally efficient and yet physically and numerically adequate model horizontal resolution is a matter of a great importance.

There are a number of studies dealing explicitly with the topic of AGCM horizontal resolution in the extended or long-range integrations. The increase in computational power has made the horizontal resolutions considered in some earlier studies to be very low by present standards (e.g. Boer and Lazare 1988). At the European Centre for Medium-Range Weather Forecasts (ECMWF), the impact of horizontal resolution on systematic errors at monthly time-scales was extensively studied by Tibaldi *et al.* (1990), comparing four different spectral resolutions: T21, T42, T63 and T106. Errors in mean fields were reduced as horizontal resolution increased. The largest differences were often found in the detailed structure of various parameters. They concluded that parameters or processes related to the representation of orography, such as precipitation, may benefit from higher model resolutions.

Williamson *et al.* (1995) found for many climate statistics a monotonic signal with increasing resolution in the NCAR model. The largest variation in these statistics was occurring at low resolutions (R15 and T21) and smallest variation occurring at medium resolutions (T42 and T63). They also found that the highest resolution does not always produce the results closest to verifying analysis. Based on integrations from an earlier version of the ECMWF model, Boyle (1993) came to similar conclusions. Phillips *et al.* (1995) ascertained that for many moist

processes, the pattern established at the T42 resolution carries over to higher resolutions with incremental variations.

Déqué and Piedelievre (1995) claim that the so-called stretched grid, of T200 over the domain of interest (Europe) and T21 over the southern Pacific, is a valid alternative to model nesting. Stratton (1999) compared the results from relatively very high horizontal resolution (0.833° latitude by 1.25° longitude) with coarser resolution in 10-year integrations of the Hadley Centre climate model (HadAM2b). She found that the increase in horizontal resolution improved the model's cold bias in the troposphere and generally increases the variability of the model. Whereas there is a general consensus that higher horizontal resolution generally has a beneficial impact on systematic model behaviour, some studies revealed problems, previously unnoticed, when the horizontal resolution was increased (e.g. Palmer *et al.* 1986).

In this paper, the effects of increasing horizontal resolution are studied using ensembles of seasonal simulations made by a relatively recent version of the ECMWF model. In the next section, a brief description of experimental strategy is given. In section 3, mean errors in upper-air fields are discussed focusing on extratropical circulation. For many parameters, *t*-test is performed to ascertain whether the ensemble mean for a given resolution is, in statistical sense, significantly different from the ensemble mean of any other resolution; these results are discussed in section 4. In section 5, some results related to the tropical large-scale circulation are presented. The impact of model resolution on precipitation and some other surface parameters is discussed in section 6 and some concluding remarks are made in section 7.

2. MODEL AND EXPERIMENTS

For the purpose of this study, the ECMWF model was integrated at T63, T_L159 and T_L319 spectral resolutions. In comparison with most previous studies in the extended-range, these resolutions, in particular T_L319, provide a substantial increase in model horizontal resolution. In the grid-point space, the T_L319 spectral resolution effectively corresponds to approximately 0.56° by 0.56° latitude/longitude grid, even higher than the one used by Stratton (1999). The numerical scheme was semi-Lagrangian, and for all resolutions, the computation in grid-point space was performed on the reduced Gaussian grid (see, for example, Hortal and Simmons 1991). The reduced grid is more isotropic in comparison to the full Gaussian grid, and performs fewer computations at middle and polar latitudes. The subscript L in T_L159 and T_L319 relates to the linear grid on which the physics parameters are computed (Hortal 1999).

The model version used for the integrations discussed in this paper was 18R6 with 31 levels in the vertical. A detailed description of major model modifications prior to this cycle is given in Gregory *et al.* (2000). This model cycle was used in ECMWF medium-range operations from June 1998 to March 1999 at the T_L319 resolution.

The 6-member ensembles were run for one summer (1987) and for one winter season (1987/88). Summer runs were initiated on and around 1 May, winter ones on and around 1 November. The initial data and sea surface temperatures (SSTs) were taken from ECMWF archive. The SSTs were updated daily in the model.

The ensemble size (6 members) used in this study was dictated primarily by computational requirements for the T_L319 resolution. However, where appropriate, for both T63 and T_L159, a brief discussion on the impact of increased ensemble size to 9 members is given. In addition, we also analysed the impact of coupling of the ECMWF wave and atmospheric models, given that the wave model is an intrinsic part of ECMWF forecasting system. For technical reasons, use of the wave model was not possible at T_L319, but the impact of the wave model at T63 and T_L159 resolutions is discussed.

For each resolution, seasonal ensemble averages were computed for conventional northern hemisphere summer, June to August (JJA), and winter, December to February (DJF), and compared with ECMWF reanalysis (ERA-15, Gibson *et al.* 1997). The spectral resolution of ERA-15 was T106. During the summer of 1987, a moderately strong El Niño event in the equatorial Pacific was observed, which subsequently weakened and almost disappeared in the following winter.

3. UPPER AIR FIELDS

Many results in this and following sections are analysed and presented in terms of ensemble mean errors with respect to ERA-15 data. Although analysis of model errors is not the main objective of this study, this approach enables assessment of relative performance of one resolution with respect to the others.

3.1 Height and wind errors

Fig.1 shows the DJF 1987/88 500 mb height ensemble mean errors with respect to ERA-15 for the three resolutions together with the reference reanalysis full field. The mainly negative mean height errors which dominate over the northern hemisphere at T63 are generally reduced at both T_L159 and T_L319 (Fig.1, left panels). This reduction is most pronounced over the Rockies and Himalayas and may be related to better representation of orography as the horizontal resolution increases.

Whereas the westerly bias over the north Pacific is monotonically reduced with resolution, over the north Atlantic and western Europe it is increased somewhat at T_L159 relative to T63, but at T_L319 reduces to become smaller than at T63. On the other hand, the amplitude of positive errors over Japan and eastern Asia increases monotonically from T63 to T_L319, though the area of error is largest at T_L159. Compared with T63, errors in the tropics and southern mid-latitudes have been also reduced in both T_L159 and T_L319 models, but increased over Antarctica (Fig.1, right panels).

Such a mixed change in error pattern with resolution is not fully understood, and one might be tempted to ascribe it to inadequate sampling. Fig.2(a) to (d) shows the DJF 1987/88 500 mb height mean errors for T63 and T_L159 respectively when ensemble size was increased from 6 to 9 members. For both resolutions, although the (northern hemisphere) mean errors are in general slightly reduced when ensemble size increases, the mean response remains essentially unchanged (cf. Fig.1(a) to (d)).

In JJA 1987, the dominant negative error over Antarctica at T63, and to a lesser extent at T_L159, has been replaced by relatively large positive error at T_L319 (not shown). It is not clear whether this change in the sign of the T_L319 error over Antarctica could be solely ascribed to a higher orography with T_L319 in comparison with the other two

resolutions. The differences between T_L319 and T_L159 orographies are mainly of the small spatial scale and are confined to the Antarctica coastal regions with the maximum difference of around 500 m on the Antarctica peninsula (60°W). In the tropics, T_L159 exhibits largest positive errors among the three resolutions.

Errors in zonally averaged zonal wind (u-wind) are shown in Fig.3. In the northern winter, errors are reduced as the model resolution increases (left panels), while in the southern winter, errors worsen with the resolution (right panels). An increase in the near tropopause errors with resolution can also be seen in the tropics during JJA. At T_L319, this deterioration of the tropical u-wind error is associated with an increase in easterlies near the tropopause. A large positive JJA error between 25°S and 45°S, found in all resolutions, is related to an erroneous overestimation of the subtropical jet by nearly 15%. It is interesting to note that, despite this increase in zonally averaged u-wind error with resolution in the southern subtropics, the longitudinally-varying u-wind error at 200 mb is largest at T63 (21 ms^{-1}), and smallest at T_L319 (16 ms^{-1}; not shown).

The underestimation of (zonally averaged) eddy kinetic energy found in earlier versions of ECMWF low resolution models (as reported in, for example, Tibaldi *et al.* 1990) is also found at T63 in both hemispheres and both seasons (Fig.4). In the northern hemisphere, this deficiency is gradually reduced as the model resolution increases. In the southern hemisphere, eddy kinetic energy is too large at T_L319 relative to ERA-15, the maximum error being confined to midlatitudes. The energy increase in T_L319 is larger in the southern summer (DJF) than in winter.

3.2 Frequency of blocking

In Fig.5(a), the wintertime (DJF) northern hemisphere frequency of blocking occurrence for the three resolutions is shown. For the definition of blocking and frequency of occurrence, the same criteria as in Tibaldi and Molteni (1990) were used. The model results are compared among themselves rather than against ERA-15, since observed blocking frequency for only one non-ENSO winter is not representative of climatological blocking frequency.

In all models, the peak frequencies for Atlantic/European block are found further east from its climatological maximum (cf. Tibaldi and Molteni 1990). A very likely cause for such a downstream displacement, in particular in the winter when blocking frequency is relatively low, is the non-negligible westerly bias over the north Atlantic discussed above. No major differences among the models are seen, though the higher resolutions tend to produce blocks over a larger geographical (longitudinal) area than T63.

Over the Pacific, blocking frequency at T63 and T_L319 is about twice as large as with T_L159. When the ensemble size is increased to 9 members, the frequency of blocks at T_L159 increases a little, but is still below the other resolutions (Fig.5(b)). It is not clear what may have caused such behaviour at T_L159. For T63 simulations, no major effects on blocking frequency due to increased ensemble size are found.

The difference in the positioning of the T63 and T_L319 Pacific blocking might be attributed to a better representation of the Rocky mountains in the highest resolution model. The ridge over the Rockies is stronger at T_L319 than at T63 (not shown, but cf. Fig.1 where the 500 mb height error over the Rockies is greatly reduced

at T_L319). This stronger ridging at T_L319 causes the upstream flow over the eastern extratropical Pacific to be more diffluent than at T63. Consequently, such a stronger diffluence may effect more favourable conditions for blocking development than relatively strong zonal flow seen at T63.

3.3 Temperature errors

An erroneous northern wintertime cooling of the high latitude troposphere is gradually reduced from T63 to T_L319, but remains almost unchanged in the polar stratosphere (Fig.6 left). In northern summer, the largest erroneous warming is found at T_L319 in the lower troposphere (Fig.6 right). Thus, in both seasons, there seems to be a monotonic increase in the northern hemisphere lower tropospheric temperature as the model resolution increases. Whereas this has a beneficial effect on mean error in northern winter, it causes the deterioration of temperature error in northern summer. Similar behaviour is also seen in the southern hemisphere, however, with a smaller amplitude.

The warming of the troposphere with increasing resolution has been also noted in some other studies, for example, Stratton (1999), Williamson *et al.* (1995). Stratton (1999) attributes the effect to the increased intensity of the hydrological cycle at higher resolution due to more intense vertical motion (see comments on precipitation changes below).

It is not clear whether an erroneous warming at low levels in JJA could be linked to land surface processes. For example, at 850 mb, temperature errors are almost equally spread over both land and sea (sea-ice) points of the northern hemisphere high latitudes (not shown). Changes to cloud amounts might be thought to play a role, but low-level cloud amounts are similar at all resolutions over the high latitudes of the northern hemisphere. For mid-level clouds, a decrease in cloud amount in this region is found as resolution increases. Errors in the poleward eddy heat flux in both winter hemispheres are lowest with T_L319 in mid-latitudes, the region where this flux is strongest (not shown).

The left panels in Fig.6 (DJF) also indicate a strong stratospheric cooling in both southern and northern high latitudes. The spatial extent of this erroneous cooling is clearly seen at 200 mb (Fig.7). At T_L319, the maximum error reaches -9 K over Antarctica, whereas at lower resolutions it is about -10 and -7 K respectively. In the northern hemisphere, the high resolution model displays the largest negative stratospheric errors. Thus, in contrast to the lower troposphere, there is a net upper air cooling as the model resolution increases (cf. Fig.6 left). This strong stratospheric cooling was also evident in the earlier versions of ECMWF model (Branković and Molteni 1997), and indeed is found to be a common deficiency of many GCMs (Boer *et al.* 1991). Johnson (1997) describes this cold bias as a means for balancing entropy in the model atmosphere since spurious numerical dispersion/diffusion, Gibbs oscillation, errors in parametrization and other improperly modelled processes cause positive "aphysical" sources of entropy.

The relative similarity in the northern hemisphere temperature error pattern between T63 and T_L159 seen in Fig.7, and somewhat different (larger) errors in T_L319, indicate a possible problem in the testing methodology adopted at ECMWF for the medium-range (see Gregory *et al.* 2000 for details). Development testing at lower resolution (T63) may not be appropriate, at least for physical parametrization, to ensure improved performance at higher resolutions.

Large positive errors in middle and low latitudes at T63 and T_L159, seen in Fig.7, can be associated with the main large-scale orography features, the Rockies and the Tibetan plateau. However, the feature that may correspond to the Andes is conspicuously absent here (nor is seen in JJA, the southern winter counterpart). In T_L319, these errors are reduced and confined mainly to the tropics and do not seem to be related to orography.

In JJA, in all resolutions considered, positive errors at 200 mb are dominant in the tropical regions (not shown). These positive errors are largest with T_L319. In mid and high latitudes negative errors of up to -9 K prevail in all resolutions (see also Fig.6 right panels).

3.4 The impact of the wave model

As indicated in introduction, for lower resolution models, T63 and T_L159, ensembles of experiments were created in which the ECMWF wave model was coupled to the atmospheric model. Here a brief summary of the impact of the wave model is given, focusing on 6-member ensembles.

Fig.2(e) to (h) shows the DJF 1987/88 500 mb height mean errors for T63 and T_L159 when the wave model was coupled to the atmospheric model. When compared with runs without wave model (Fig.1(a) to (d)), it can be seen that the inclusion of the wave model generally contributes to the reduction of error amplitude over much of the globe; however, the error pattern remains essentially unchanged. It seems that the impact of wave model coupling is more significant at T63 than at T_L159. For example, whereas at T63 the westerly bias over the north Atlantic is substantially reduced, at T_L159 it is reduced only marginally. Over Antarctica, the coupling of the wave model yields a somewhat deteriorating effect. Similar model response is found in JJA and for some other parameters. These results are consistent with those of Janssen and Viterbo (1996) who found a (mostly) beneficial impact of ocean waves on the climatology of an earlier version of ECMWF model.

4. STATISTICAL SIGNIFICANCE OF DIFFERENCES BETWEEN RESOLUTIONS

A *t*-test was performed to establish how different was the ensemble mean at one resolution when compared with the ensemble mean at the other resolutions. Fig.8 shows the DJF 500 mb geopotential height difference field together with the spatial distribution of *t*-values at the 90% confidence level when T63 and T_L159 are compared (Fig.8(a)) and when T_L159 and T_L319 are compared (Fig.8(b)). The difference fields in Fig.8 and in subsequent figures with *t*-statistics are always computed in the sense of 'lower resolution minus higher resolution'. Although the differences between T63 and T_L159 in the tropical regions (between 30^{O}N and 30^{O}S, Fig.9(a)) are relatively small when compared to the extratropics (mainly less than 2 dam), the shading indicate that in statistical sense they are highly significant. Outside the tropics there are many regions with significant differences: northern Europe and northern Asia, southern Asia, subtropical Atlantic, north-western North America and the southern Indian Ocean. Most differences are of the negative sign indicating a warming of much of the extratropical troposphere at T_L159 relative to T63; relatively large positive differences over the north Pacific are not significant.

The difference between the two higher resolutions (Fig.8(b)) is somewhat less statistically significant than that between T63 and T_L159. It is confined mainly to the tropics, the 90% confidence level being broken into several

regions indicating a less coherent difference between the two high resolutions than that between T63 and T_L159. The relatively large differences over the northern Europe and north-eastern Atlantic are also statistically significant. It is interesting to note that in both panels of Fig.8 the differences over the Tibetan Plateau are highly significant, indicating an important impact of changing orography with resolution on 500 mb height field over that region.

For JJA, similar results to those seen for DJF are evident, in particular for the T63 vs. T_L159 comparison (not shown), but some variations exist. For the T_L159 vs. T_L319 comparison the 90% significance level is found over much of the southern Asia, with differences of nearly 8 dam in the region of the Persian Gulf. However, for the T63 vs. T_L159 comparison the 90% threshold does not cover the Arabian Sea and Middle East (it is even below 80%), i.e. these two resolutions do not differ significantly over that region. This indicates relatively large differences in the representation of the Indian summer monsoon with higher resolutions. Indeed, the low level flow at 850 mb over the Arabian Sea is very similar at T63 and T_L159 (and relatively close to ERA-15), but has been strengthened at T_L319 (not shown; see also the discussion on monsoon precipitation in section 6.1). These results suggest that the resolution increase might affect different flows in different ways.

For u-wind at 200 mb, the largest differences were found between T_L159 and T_L319 in JJA over the African-Indian region (Fig.9(a)). This is the consequence of an overestimation of easterlies at T_L319; the maximum error over the eastern Africa reaches 12 ms^{-1} at T_L319 compared to a half of that amplitude at T_L159 (see also Fig.3 right panels). This is in agreement with the most intense precipitation during the Indian summer monsoon in the T_L319 model. The negative and statistically significant differences over the north Atlantic and across the central and eastern Europe in Fig.9(a) indicate a somewhat stronger and broader subtropical jet over these regions in T_L319 relative to T_L159. This has an implication on the European summer precipitation rates in the high-resolution model (see section 6.1 below).

In section 3.3, large northern hemisphere differences in temperature at 200 mb between T_L319 and other model resolutions were discussed (Fig.7). This is also seen in Fig.9(b) where these large differences between T_L159 and T_L319 (of nearly 4 K) are marked by the 90% significance level. Statistically significant differences are also found over much of the tropics and in the southern hemisphere.

5. TROPICAL CIRCULATION

In this section we focus on the dynamics of a large-scale tropical circulation. Because of its intrinsic links with other spatial scales, some of large-scale circulation effects on smaller scales will be discussed here. However, a more detailed discussion on precipitation rates and other surface parameters is given in section 6.

5.1 Vertical motion

Considering the zonal mean meridional circulation in the tropics (not shown), all the resolutions overestimate the Hadley cell relative to ERA-15. The error is largest at T63, gradually decreasing with resolution. Irrespective of season, the largest contribution to this error comes primarily from model's overestimation of the large-scale tropical ascent. However, it has to be noted that this type of error may depend to a great extent on the formulation of model physics (see, for example, Branković and Molteni 1997). The physical parametrization in the ECMWF

model has undergone a series of changes between cycle 13R4 (introduced in operations in April 1995 and used for ERA-15) and cycle 18R6 used for these experiments. Therefore, a cautious approach has to be exercised when verifying forecast data that are primarily driven by model physics.

Some details of the 500 mb spatial distribution of the tropical vertical velocity are shown in Fig.10. In DJF (left panels), the largest area of a relatively strong ascent over the Pacific warm pool region is found in T_L319. Since the SSTs were identical in all the resolutions considered, this implies that the highest resolution is reacting more strongly to the forcing from the boundary imposed by prescribed SST. In all resolutions, a narrow area of descent is seen in the central equatorial Pacific situated in between the two branches of rising motion of the inter-tropical convergence zone (ITCZ) and the south Pacific convergence zone (SPCZ) respectively, this feature being the most prominent in the T_L319 model.

As the DJF rising motion in the SPCZ becomes stronger with resolution, it also increases in the region between the northern Australia and Papua/New Guinea. Although this brings some increase in total cloudiness at T_L319 over the northern Australia, only a slight increase in monsoon precipitation occurs (not shown).

The largest discrepancy between the model simulations (regardless of the resolution) and ERA-15 in terms of the 500 mb vertical motion is found over the northern part of South America in DJF. Whereas in ERA-15 a rising motion is dominant over this region (not shown), in the model a relatively strong descent is seen (Fig.10 left). Though this descent is manifested in a somewhat reduced cloud cover, the model precipitation rate over this region as verified against the Xie-Arkin data (Xie and Arkin 1997) is reasonable, thus indicating that ERA-15 may not be reliable in this case.

In JJA (Fig.10 right panels), the T_L319 displays the most structured and detailed ascent over the Indian monsoon region, including the Bay of Bengal. However, this is not necessarily the most accurate model simulation. As discussed below, at T_L319 the Indian monsoon precipitation rates exceed substantially observed values. On the other hand, over the western equatorial Pacific, the rising motion is somewhat weakened at T_L319 when compared with both T63 and T_L159. The impact on precipitation is seen in Fig.14; at T_L319, reduced amounts of precipitation over the South China Sea are seen relative to the other resolutions.

The Atlantic ITCZ is strongest with the T_L319 resolution, as is the area of rising motion off the eastern coast of the United States, over the Gulf Stream. The latter may have important consequence on local atmospheric thermal stability that in turn may influence the maintenance and landfall of tropical cyclones in late summer.

5.2 Velocity potential and tropical variability

The large-scale tropical circulation is also shown in terms of velocity potential at 200 mb. Fig.11(a) shows the T63 full field, and Fig.11(b) and (c) shows the difference between the higher resolutions and T63 respectively. (Note that differences in Fig.11 (b) and (c) are in the opposite sense than those in Fig.8.) As for the 500 mb vertical velocity above, the results in Fig.11 do not refer to ERA-15. Tropical precipitation appears to be sensitive to horizontal resolution (see section 6.1 below), and the ECWMF convection scheme has undergone a major change

from the time when ERA-15 data were made (see, for example, Gregory *et al.* 2000). Therefore, velocity potential from ERA-15 may not be reliable for the verification when horizontal resolution is changed in the model.

We focus on the summer season, because the Walker circulation is, to a certain extent, related to the strength of the Indian monsoon. A negative difference over the south Asia indicates an increase in the maximum of upper air divergence at T_L159 and T_L319 relative to T63 with the outflow being much stronger at T_L319 than at T_L159. This may be symptomatic of the model being over-responsive to SST anomalies of JJA 1987, in particular at higher resolutions (cf. similar result for an earlier version of ECMWF model in Palmer *et al.* 1992). The centre of the upper-air convergence has been strengthened and expanded from South America towards the African continent, again much more intense at the highest resolution. Overall, although the pattern of the modelled large-scale tropical circulation is consistent among the resolutions considered, its intensity becomes larger as resolution increases.

The tropical (total) variability is also affected by the change in horizontal resolution. Fig.12 shows standard deviation of the 850 mb relative vorticity for JJA for the three resolutions and ERA-15. While Gregory *et al.* (2000) indicate uncertainty in the use of this quantity diagnosed from ERA-15, in that it may underestimate tropical variability, the T63 model, and to a lesser extent T_L159, clearly underestimate variability in the low-level vorticity field. Although at T_L319 there are some disagreements in details with ERA-15, the overall representation of variability over much of the tropics is definitely improved over the lower resolutions. For DJF, similar results are found (not shown).

Previous studies have found that tropical variability is sensitive to the nature of the convection scheme (see, for example, Slingo *et al.* 1994, Gregory *et al.* 2000). These studies suggested that the comparison between simulated and analysed measures of variability is a useful indication whether the performance of the convection scheme is reasonable. However, they used resolution of T63 or lower, and a large sensitivity of simulated tropical variability to increasing resolution demonstrated in Fig.12 suggests that care must be exercised when interpreting the nature of such studies.

The day-to-day variability of the 200 mb velocity potential during the DJF 1987/88 season was also analysed by using Hovmöller diagrams. This diagnostic is representative of the Madden-Julian oscillation (MJO; Madden and Julian 1971). In the verifying analysis, the two bursts of the upper-air divergent outflow can be identified moving eastward between 45°E and 150°E over the period of approximately 40 days (not shown). Neither resolution was able to reproduce this type of variability in the large-scale tropical flow. This result suggests a requirement, irrespective of horizontal resolution, for further reduction of model tropical errors before reliable tropical intraseasonal variability can be attained.

6. SURFACE FIELDS

6.1 Precipitation

Fig.13 shows seasonal mean precipitation in $mmday^{-1}$ for DJF (left) and JJA (right) over the European region. For both seasons, a gradual increase in precipitation amounts as the resolution increases is seen. This is evident almost all over the continent and parts of eastern Atlantic. Such an increase in precipitation can be in many places related

to a better resolved orographic features (e.g. the Alps, the Caucasus, the Norwegian, Scottish and Albanian mountains). However, it is also seen in some areas where orography is either featureless or nonexistent (e.g. eastern Europe, Finland, Russia, the North Sea).

In both seasons, the large-scale precipitation is the main contributor to such an overall precipitation increase (not shown), convective precipitation contributes comparatively much less. In DJF, slightly more than 2 mmday^{-1} over the Atlantic and the Mediterranean is convective in nature, whilst in JJA, convective precipitation contributes over the continental region only and is more widespread at T63 than at T_L319 resolution. The latter indicates the refinements and inclusion of relatively small-scale features in the representation of orography at T_L319. An increase in the JJA total precipitation at T_L319 relative to T_L159 over some parts of Europe is consistent with a relative strengthening of the subtropical jet (and the Atlantic storm track) in the high resolution model (see section 4 and Fig.9(a)).

The increase in precipitation with resolution has been also noted in some previous studies, for example, Jones *et al.* (1995) and Stratton (1999). In the former, a regional climate model of similar resolution to T_L319 covering the eastern north Atlantic and Europe was compared to a low-resolution climate model. The increase in precipitation was attributed to a larger vertical velocity at higher resolution. This is consistent with increased low-level moisture convergence. The additional effect of such an intensified hydrological cycle was also seen in increased tropospheric temperatures (cf. our discussion in section 3.3 above).

In our experiments, the southern branch of the DJF 850 mb moisture flux, which penetrates from the Atlantic into Spain and further over the southern Europe, the Mediterranean and into the Black Sea is strongest in the T_L319 ensemble (not shown). The northern branch, which forks before the Alps from its southern counterpart into the central and northern Europe, is very similar in all resolutions. However, at T_L319 a somewhat stronger moisture flux *convergence* over the eastern Europe may have contributed to a larger precipitation rates in that region when compared with the other two resolutions. In JJA, the 850 mb moisture flux over the central and eastern Europe is again strongest at T_L319 and may be linked with increased precipitation there.

For the verification of precipitation the data of Xie and Arkin (1997) were used. Seasonal averages were derived from monthly means for appropriate years. Whereas in DJF the T63 and T_L159 resolutions are relatively close to the verification data, with a drier eastern Europe and a wetter western Europe, in JJA, the T_L319 seems to fit best these verification estimates (not shown).

Considering the Asian subcontinent, the maximum in the monsoon precipitation over the western India and the Bay of Bengal is doubled at T_L319 when compared with T63 (Fig.14). Such a substantial increase may be ascribed to both better resolved orographic effects of the Western Ghats and an enhancement of the low level jet off the Somali coast in T_L319 (not shown; but see discussion in section 4 above). When compared with the Xie-Arkin data, all resolutions overestimate Indian rainfall. On the other hand, in the Bay of Bengal, T63 underestimates, T_L319 overestimates, and T_L159 gives about right amount of precipitation.

The zonally averaged precipitation in both seasons, for both model and Xie-Arkin precipitation data, is shown in Fig.15. The T_L319 exhibits the largest zonally averaged precipitation rates of all resolutions. In midlatitudes, the difference between T_L319 and the other resolutions amounts up to 1 mmday^{-1}. A relatively large difference in the belt between the equator and 10-15°S is mainly due to an increase in the SPCZ rainfall in the highest resolution model. A relatively good agreement among the models is found in high latitudes and during JJA in the region of ITCZ. The Xie-Arkin precipitation is consistently lower when compared with the model. The largest discrepancy between the model and verification can be seen in winter midlatitudes - up to 2 mmday^{-1} for T_L319. All resolutions overestimate precipitation in the ITCZ, particularly in DJF. The consistency among resolutions and the agreement between the model and verification data is improved when only land points are considered (not shown). This may indicate that better representation of modelled precipitation is linked to orographic features.

The *t*-statistic, discussed in section 3.4 for upper-air fields, was also computed for precipitation. Irrespective of season, statistically significant differences between T63 and T_L159 resolutions are found mainly in the tropical and subtropical regions, in particular in the eastern Pacific off the coasts of Central and South America (not shown). The latter is associated with low stratiform cloud decks and very little or no precipitation; small increases in cloud cover at T_L159 and negligible increases in precipitation contribute to high *t*-values over these regions. The significant differences between T_L159 and T_L319 are more widespread, and in addition to the tropics cover many parts of the extratropics, such as, the northern and southern storm track regions.

In Fig.16 the *t*-statistic and precipitation differences are shown for the Indian summer monsoon (left) and for Europe in DJF (right). As before, the 90% confidence level is shown in both regions. Apart from the Himalayas and Tibetan Plateau, the largest and statistically significant precipitation differences in the Indian monsoon region, for both pairs of resolutions, are found over the Arabian Sea and the Bay of Bengal and adjacent coastal areas. The differences in the inner India are not statistically significant, though they reach locally up to 5 mmday^{-1}. On the other hand, the higher rainfall amounts along the equator produced by the T63 resolution are significantly different from those found at T_L159.

Over Europe, the T63 vs. T_L159 comparison yields, in general, relatively little statistical significance. For T_L159 vs. T_L319 comparison, greater winter precipitation with the higher resolution is significant over much of the continent. However, this should not be considered to be only caused by a better representation of orography at T_L319 - shaded areas being also found over the Atlantic and much of the eastern European flatlands (see also discussion above).

6.2 Surface fluxes and wind stress

The net surface thermal balance over sea points changes little as the resolution increases. In DJF, the heat deficit is 12.5, 10.1 and 11.6 Wm^{-2} for T63, T_L159 and T_L319 respectively; in JJA, a heat surplus of 18.9, 21.2 and 23.9 Wm^{-2} respectively is seen. This small variation across different resolutions is somewhat misleading, since for T_L319 a strong compensating effect between different components takes place. At T_L319, both surface latent heat flux and thermal radiation (both mainly negative) and surface solar radiation (mainly positive) exhibit an increase in amplitude relative to the lower resolutions. The only component of the thermal balance that remains essentially unchanged at T_L319 when compared with the other resolutions is surface sensible heat flux. Therefore, the overall

effect of these (opposite) flux increases at T_L319 is that the net surface flux at the highest resolution is rather similar to that at T63 and T_L159.

The DJF surface wind stress in the north Pacific winter storm track is monotonically enhanced from T63 to T_L319 (Fig.17). However, this is not the case in the region of trade winds. In both northern and southern trades, wind stress is reduced at T_L159 relative to T63. At T_L319, surface wind stress is increased in the southern trades again. Similar behaviour is also found in the Indian ocean in both seasons. This increase in surface wind stress at T_L319 is associated with an increase in (oceanic) surface evaporation rates relative to the other resolutions (not shown).

7. CONCLUSIONS

The impact of horizontal resolution on seasonal timescales has been studied from ensembles of integrations made with a relatively recent version of the ECMWF model. The model was integrated at T63, T_L159 and T_L319 spectral resolution; the latter effectively corresponds to 0.56° latitude/longitude grid. The 6-member ensembles were run for one winter and one summer season. Whereas one winter and one summer are by no means sufficient to evaluate model biases fully, they nevertheless give a valuable insight on the influence of horizontal resolution on seasonal timescales.

The general impression is that there are no dramatic differences in simulated ensemble averages among the three resolutions considered, i.e. for most parameters, circulation and error patterns are similar. Also, no clear pattern of either improvement or deterioration emerged as the horizontal resolution changes. However, differences among the resolutions exist and are mostly in the detail rather than characterising the large-scale flow. In some cases a direct relationship between improved representation of orography, as the horizontal resolution increases, and changed circulation feature can be concluded (like increased winter precipitation rates over Europe). However, some differences cannot be always attributed to local differences in the representation of orography. Overall, the upper-air fields seem to benefit most from increased horizontal resolution. However, it is not clear if this is the case for surface fields.

Whereas some changes in model response are not monotonic with the resolution increase from T63 to T_L159 and to T_L319, there are some systematic changes with resolution, especially in the tropics. These systematic differences between various resolutions question whether it is sufficient to rely solely on low-resolution simulations for model development and testing, a common practice adopted by many modelling centres.

As already noted by Williamson *et al.* (1995), increased resolution does not always lead to improved results. The prime example in this study is Indian summer monsoon precipitation - at T_L319 it substantially overestimates observational data. On the other hand, whereas reanalysis data (either from ERA or other reanalyses) are invaluable for assessment of various aspects of model climatology, not all parameters from reanalyses are reliable for verification purposes. For example, vertical velocity depends strongly on model physical formulation, and so verification of a different version of the same model with reanalysis data may lead to erroneous conclusion about model systematic error.

Acknowledgement: We thank Nils Wedi for his help in setting up and running the T_L319 resolution experiments and Laura Ferranti for producing the MJO diagnostics. Comments and suggestions by Martin Miller and Tim Palmer are highly appreciated.

References

Boer, G.J. and M. Lazare, 1988: Some results concerning the effect of horizontal resolution and gravity-wave drag on simulated climate. *J. Climate*, **1**, 789-806.

Boer, G.J., K. Arpe, M. Blackburn, M. Déqué, W.L. Gates, T.L. Hart, H. Le Treut, E. Rockner, D.A. Sheinin, I. Simmonds, R.N.B. Smith, T. Tokioka, R.T. Wetherald and D. Williamson, 1991: An intercomparisonof the climates simulated by 14 atmospheric general circulation models. CAS/JSC Working Group on Numerical Experimentation, Rep. 15, WMO/TD-No.425.

Boyle, J.S., 1993: Sensitivity of dynamical quantities to horizontal resolution for a climate simulation using the ECMWF (cycle 33) model. *J. Climate*, **6**, 796-815.

Branković, Č. and F. Molteni, 1997: Sensitivity of the ECMWF model northern winter climate to model formulation. *Clim. Dyn.*, **13**, 75-101.

Déqué, M. and J.Ph. Piedelievre, 1995: High resolution climate simulation over Europe. *Clim. Dyn.*, **11**, 321-339.

Gibson, J.K., P. Kållberg, S. Uppala, S. Nomura, A. Hernandez and E. Serrano, 1997: *ERA description.* ECMWF Re-Analysis project Report Series No. 1.

Gregory, D., J.-J. Morcrette, C. Jakob, A. Beljaars and T. Stockdale, 2000: Revision of convection, radiation and cloud scheme in the ECMWF Integrated Forecasting System. To appear in *Q. J. R. Meteorol. Soc.* (also ECMWF Tech. Memo. 254)

Hortal, M., 1999: The development and testing of a new two-time-level semi-Lagrangian scheme (SETTLS) in the ECMWF forecast model. ECMWF Tech. Memo. 292.

Hortal, M. and A.J. Simmons, 1991: Use of reduced Gaussian grids in spectral models. *Mon. Wea. Rev.*, **119**, 1057-1074.

Janssen, P.A.E.M. and P. Viterbo, 1996: Ocean waves and the atmospheric climate. *J. Climate*, **9**, 1269-1287.

Johnson, D.R., 1997: "General coldness of climate models" and the second law: Implictions for modeling the Earth system. *J. Climate*, **10**, 2826-2846.

Jones, R.G., J.M. Murphy and M. Noguer, 1995: Simulation of climate change over Europe using a nested regional-climate model. I: assessment of control climate, including sensitivity to location of lateral boundaries. *Q. J. R. Meteorol. Soc.*, **121**, 1413-1449.

Madden, R.A. and P.R. Julian, 1971: Detection of a 40-50 day oscillation in the zonal wind in the tropical Pacific. *J. Atmos. Sci.*, **28**, 702-708.

Palmer, T.N., Č. Branković, P. Viterbo and M.J. Miller, 1992: Modelling interannual variations of summer monsoons. *J. Climate*, **5**, 399-417.

Palmer, T.N., G.J. Shutts and R. Swinbank, 1986: Alleviation of a systematic westerly bias in general circulation and numerical weather prediction models through an orographic gravity wave drag parameterisation. *Q. J. R. Meteorol. Soc.*, **112**, 1001-1039.

Phillips, T.J., L.C. Corsetti and S.L. Grotch, 1995: The impact of horizontal resolution on moist processes in the ECMWF model. *Clim. Dyn.*, **11**, 85-102.

Slingo, J.M., M. Blackburn, A. Betts, R. Brugge, K. Hodges, B. Hoskins, M. Miller, L. Steenman-Clark, and J. Thurburn, 1994: Mean climate and transience in the tropics of the UGAMP GCM: Sensitivity to convective parametrization, *Q. J. R. Meteorol. Soc.*, **120**, 881-922.

Stratton, R.A., 1999: A high resolution AMIP integration using the Hadley Centre model HadAM2b. *Clim. Dyn.*, **15**, 9-28.

Tibaldi, S. and F. Molteni, 1990: On the operational predictability of blocking. *Tellus*, **42A**, 343-365.

Tibaldi, S., T.N. Palmer, Č. Branković and U. Cubasch, 1990: Extended-range predictions with ECMWF models: Influence of horizontal resolution on systematic error and forecast skill. *Q. J. R. Meteorol. Soc.*, **116**, 835-866.

Williamson, D.L., J.T. Kiehl and J.J. Hack, 1995: Climate sensitivity of the NCAR Community Climate Model (CCM2) to horizontal resolution. *Clim. Dyn.*, **11**, 377-397.

Xie, P. and P. A. Arkin, 1997: Global precipitation: a 17-year monthly analysis based on gauge observations, satellite estimates and numerical model outputs. *Bull. Amer. Meteo. Soc.*, **78**, 2539- 2558.

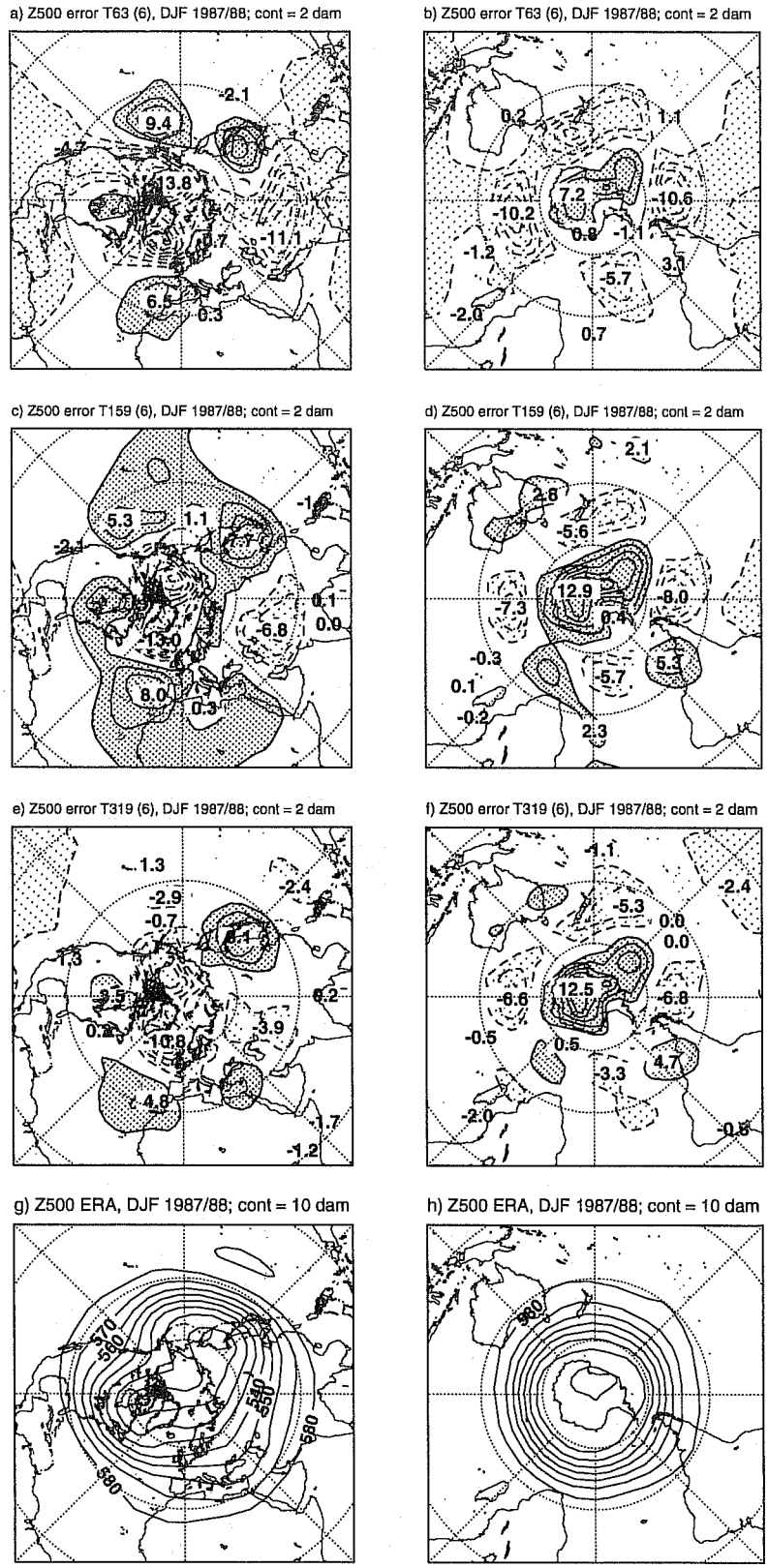

Fig.1 DJF 1987/88 ensemble mean 500 mb geopotential height error fields for T63: (a) and (b), for T_L159: (c) and (d), for T_L319: (e) and (f), and ERA-15 full field: (g) and (h). Contours 2 dam for error fields and 10 dam for the full field. Positive errors dense stipple, negative errors coarse stipple.

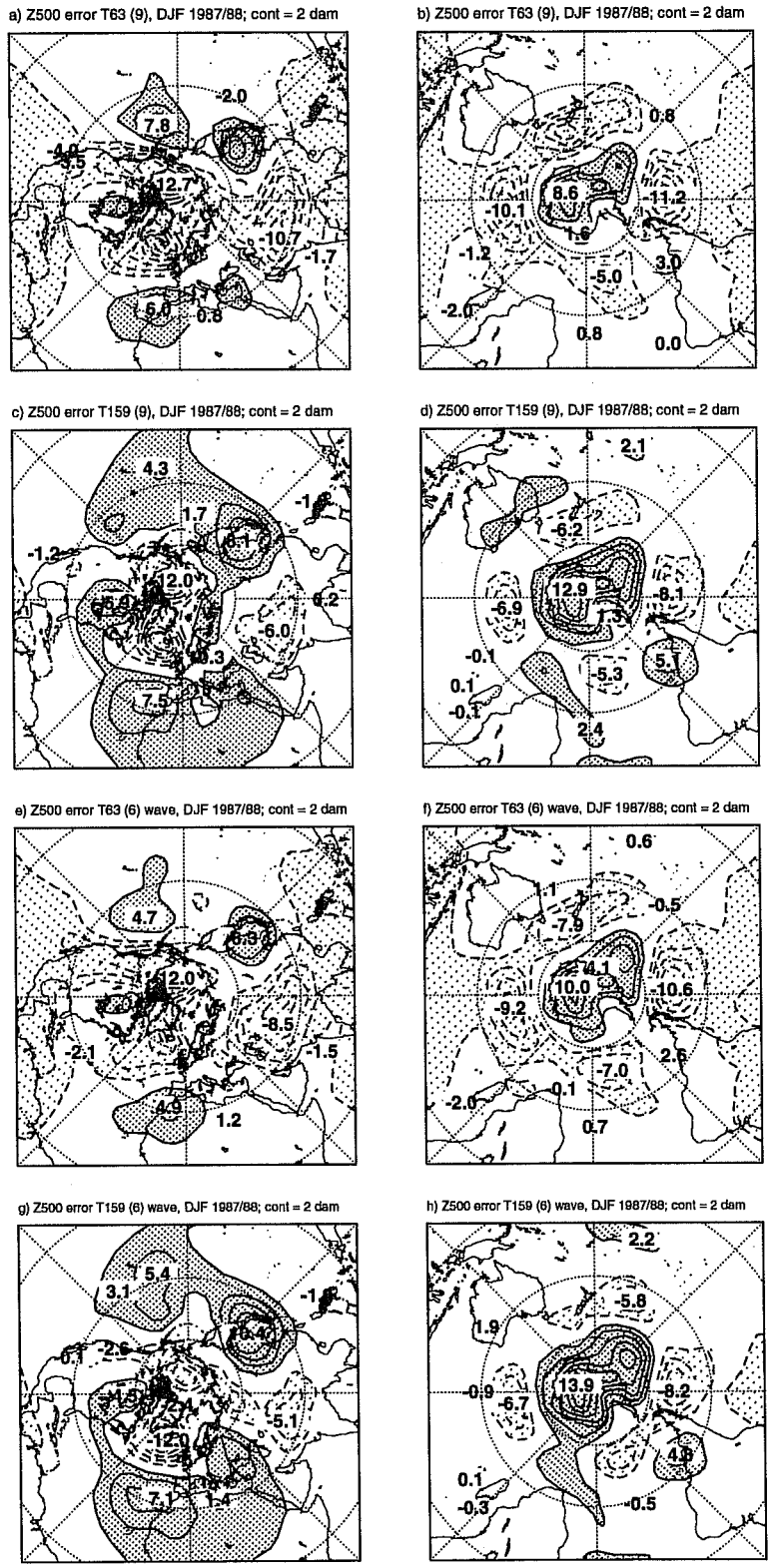

Fig.2 As Fig.1, but when ensemble size was increased to 9 members for T63: (a) and (b), for T_L159: (c) and (d); when wave model was coupled to the atmospheric model for T63: (e) and (f), and for T_L159: (g) and (h). Contours 2 dam, positive errors dense stipple, negative errors coarse stipple.

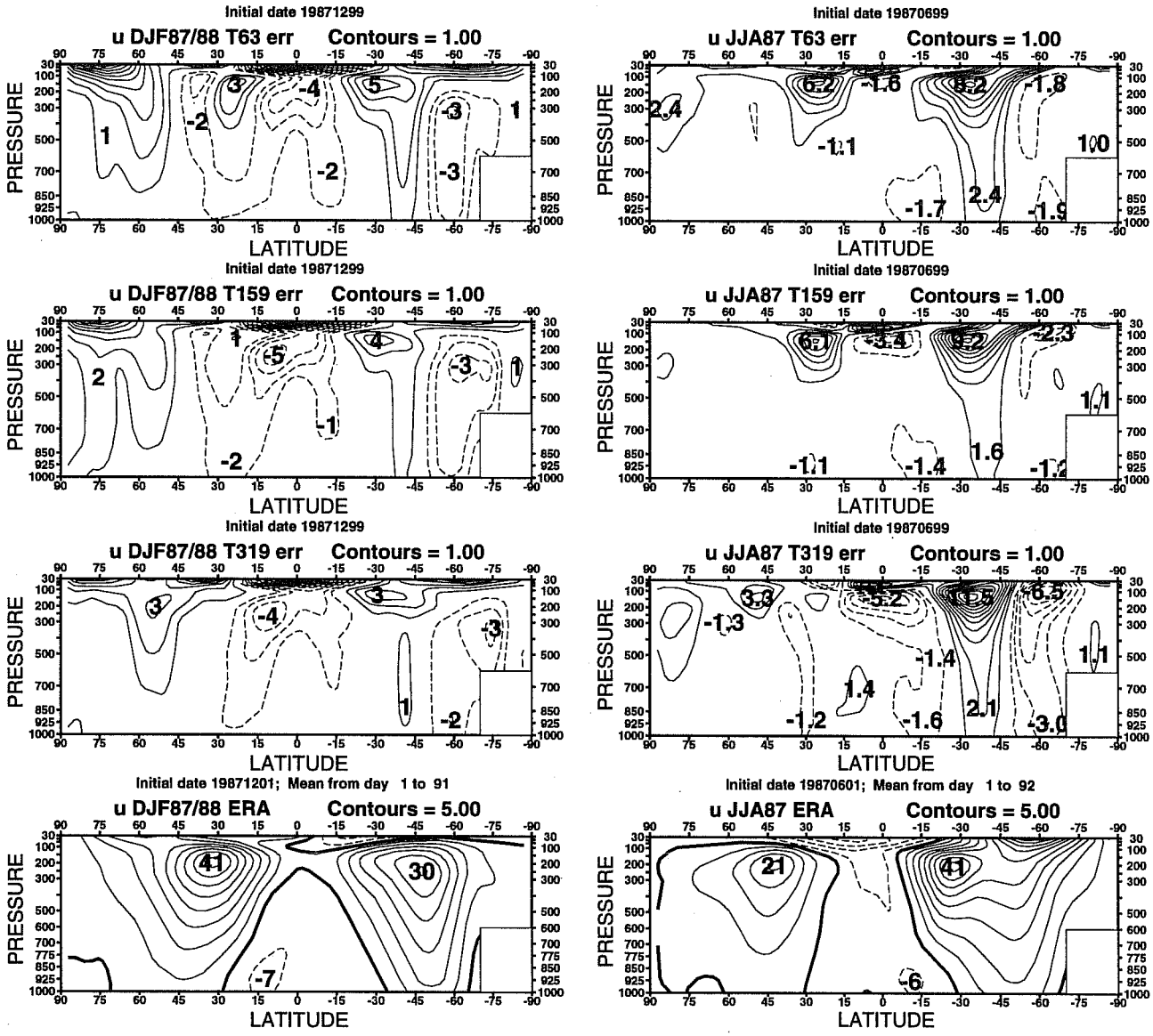

Fig.3 Zonally averaged u-wind ensemble mean errors for DJF 1987/88 (left) and JJA 1987 (right). From top to bottom: T63, T_L159, T_L319 errors respectively and ERA-15 full field. Contours 1 ms^{-1} for errors and 5 ms^{-1} for full fields. Negative errors and easterlies dashed.

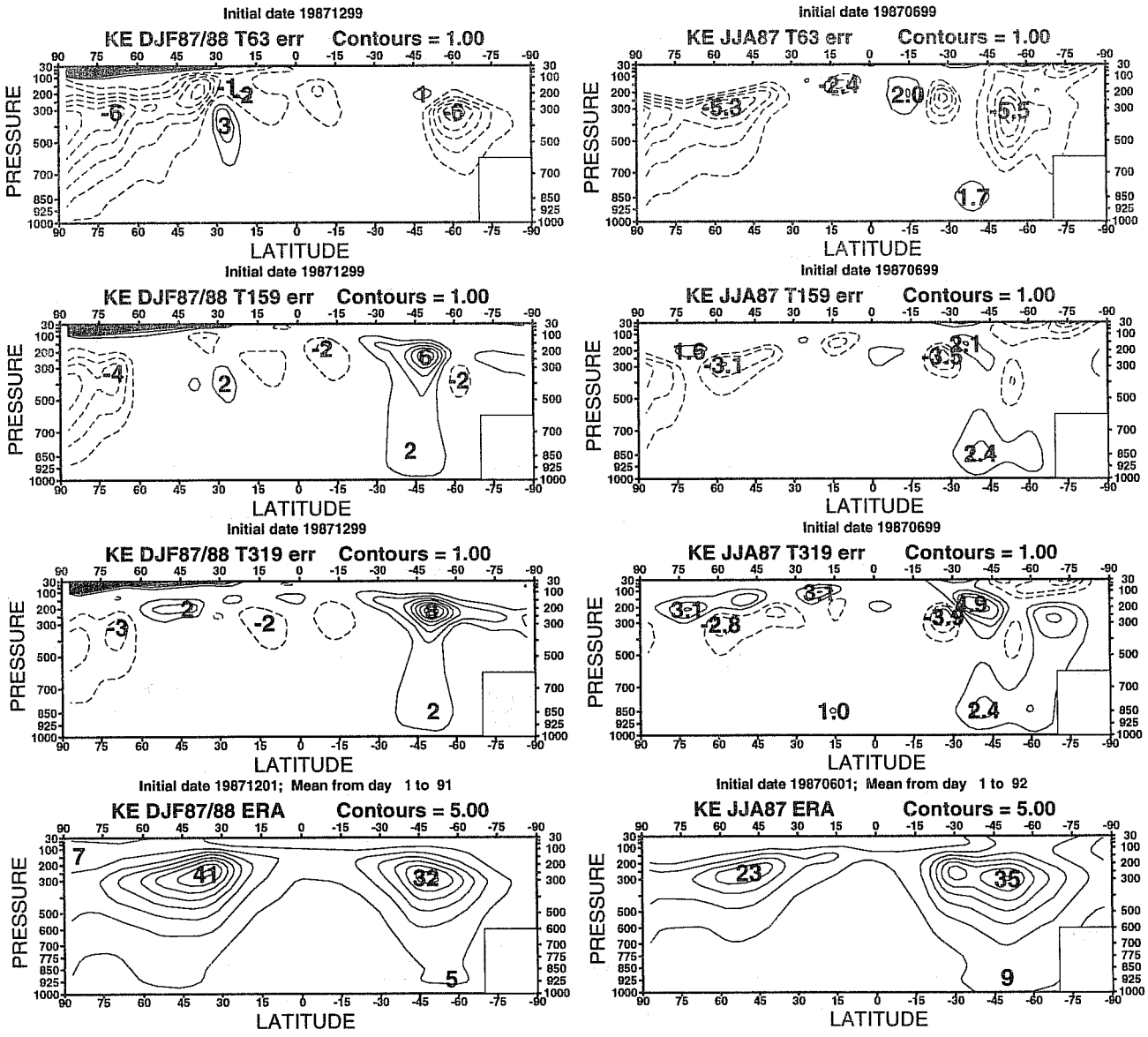

Fig.4 As Fig.3 but for eddy kinetic energy. Units are J/(m²Pa). Negative errors dashed.

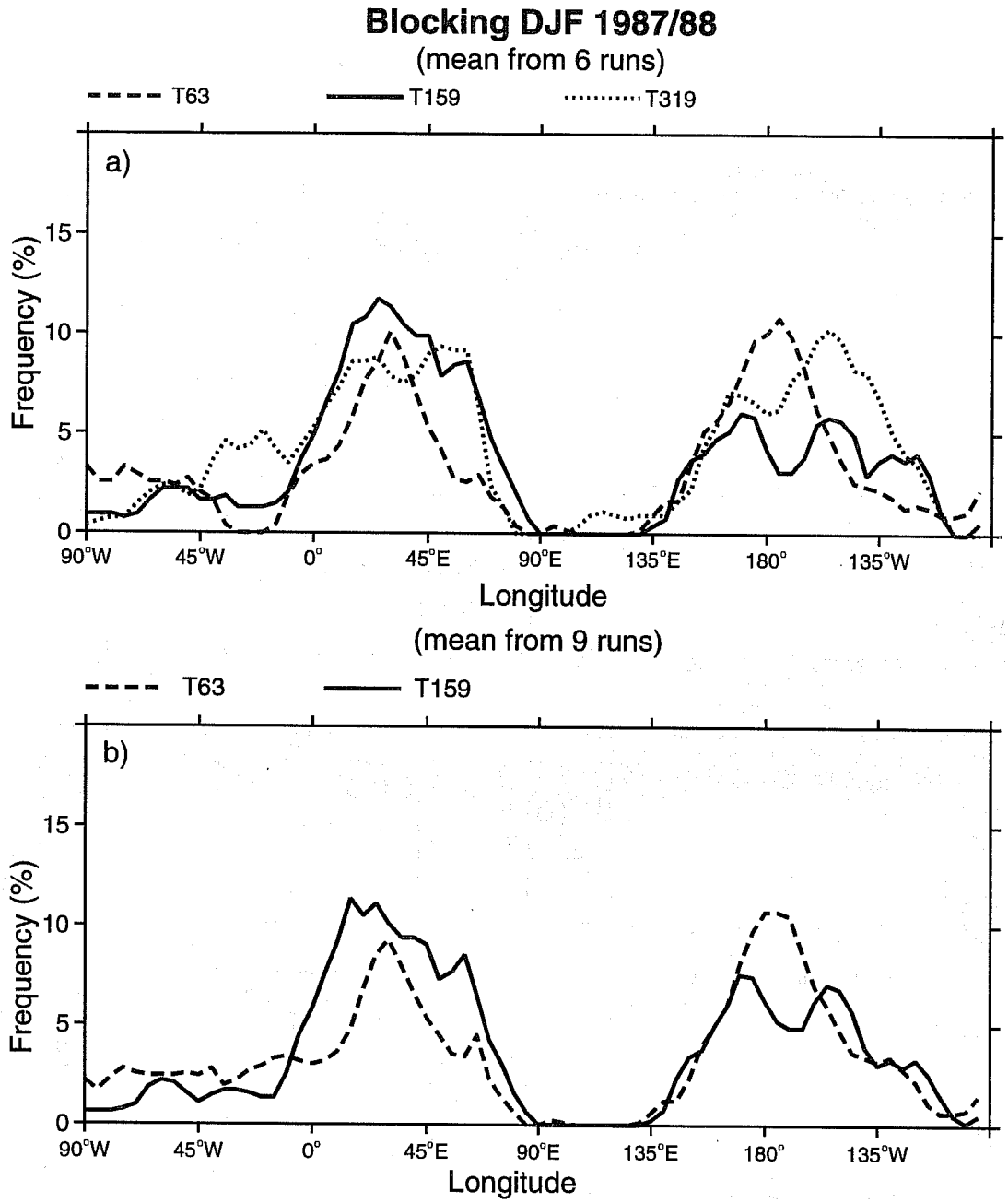

Fig.5 Frequency of blocking occurrence in % in DJF 1987/88 for (a) 6-member ensembles for T63 (dashed), T_L159 (solid) and T_L319 (dotted) resolutions, and (b) 9-member ensembles for T63 and T_L159.

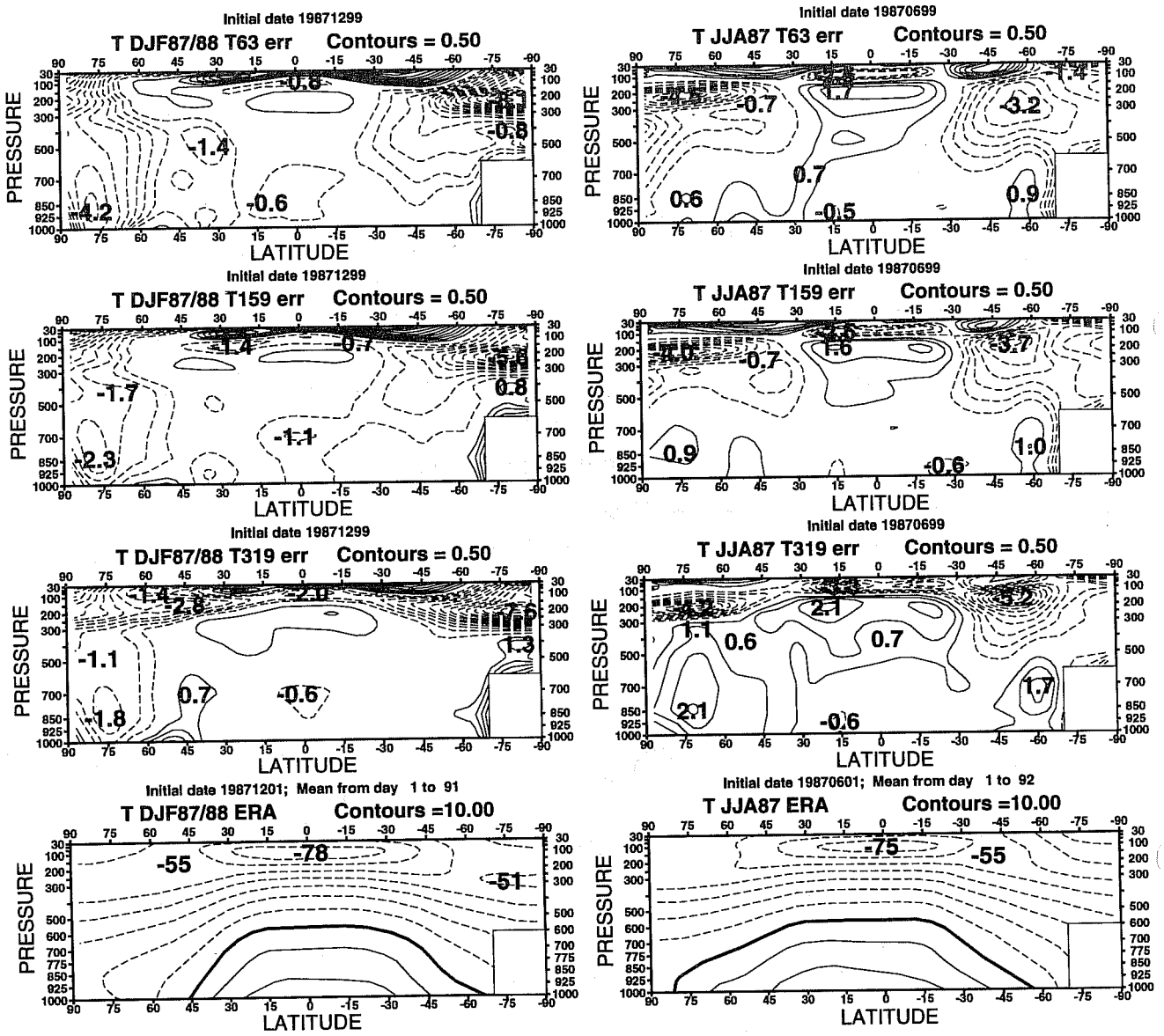

Fig.6 Same as Fig.3 but for temperature. Contours 0.5 K for errors and 10 K for full fields. Negative errors and negative temperatures dashed.

a) T200 error T63 (6), DJF 1987/88; contours = 1 deg

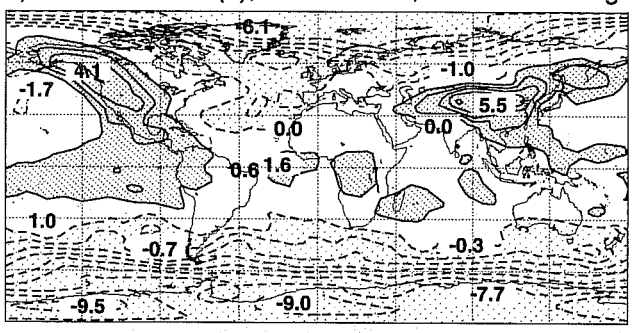

b) T200 error T159 (6), DJF 1987/88; contours = 1 deg

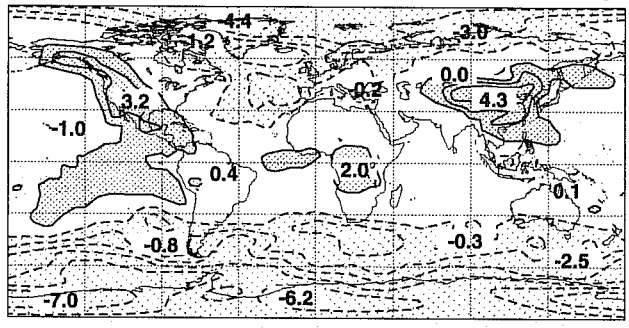

c) T200 error T319 (6), DJF 1987/88; contours = 1 deg

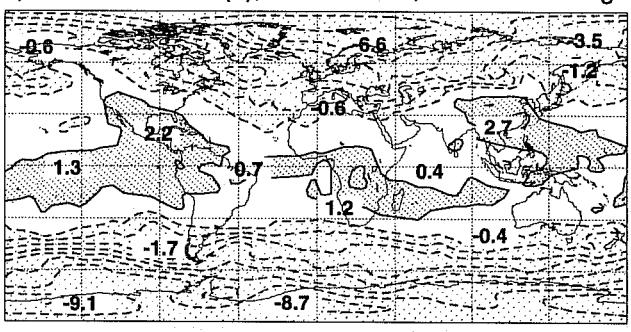

d) T200 ERA-15, DJF 1987/88; contours = 2 deg

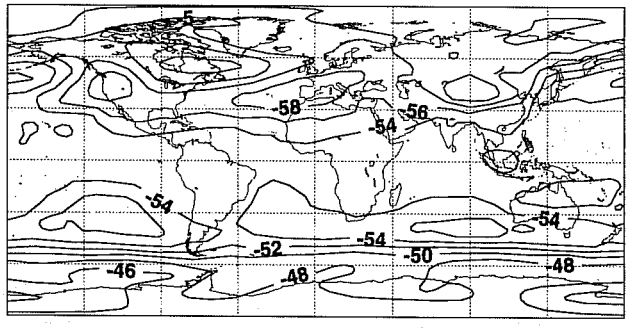

Fig.7 As Fig.1 but for the DJF 1987/88 200 mb temperature. Contours 1 K for error fields and 2 K for the full field.

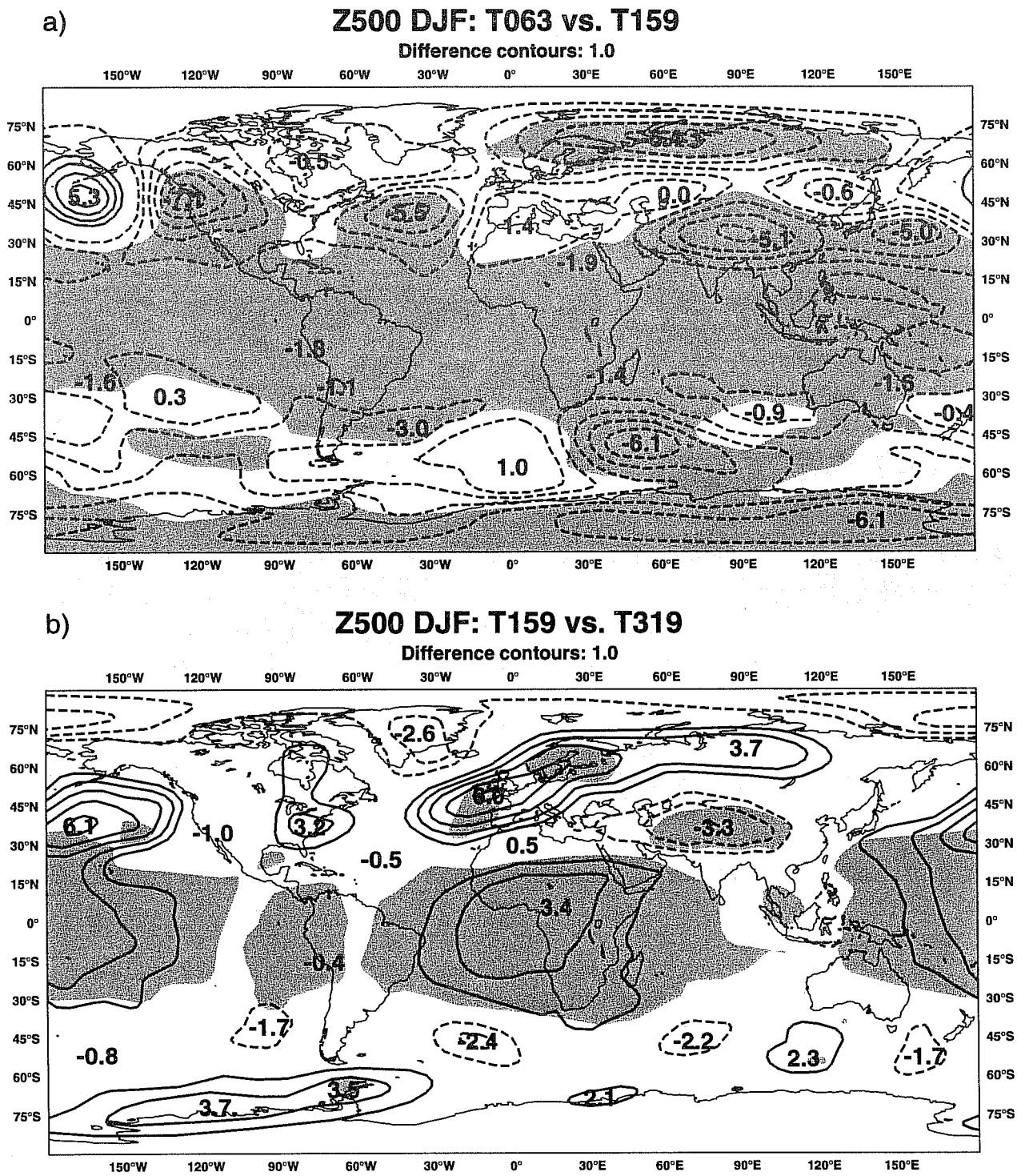

Fig.8 Differences and *t*-statistic of the DJF 1987/88 500 mb geopotential height for the comparison of (a) T63 minus T_L159, and (b) T_L159 minus T_L319. Difference contours 1 dam; negative differences dashed. Shading for 90% confidence level.

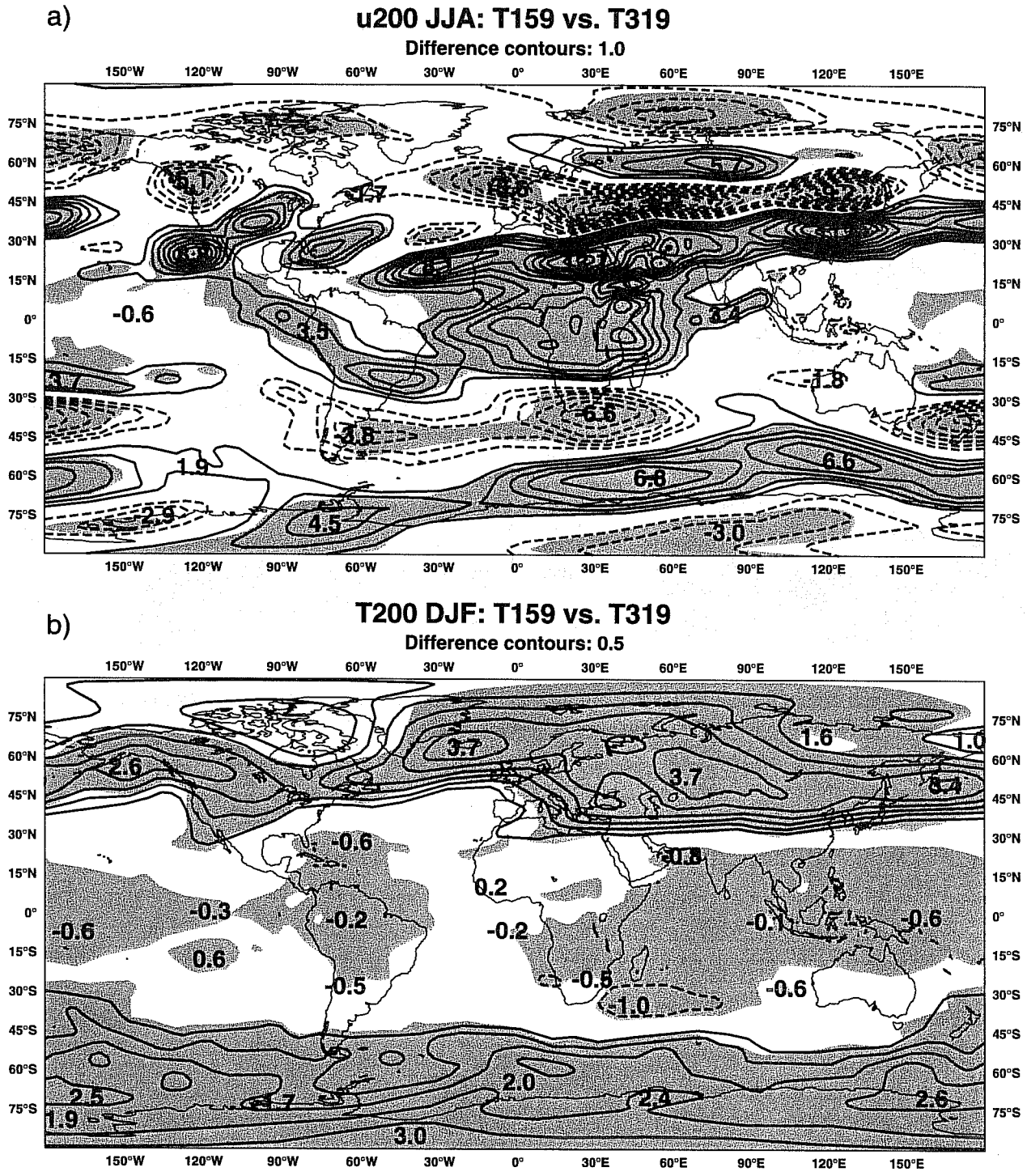

Fig.9 As Fig.8 but for the comparison of T_L159 minus T_L319 for (a) JJA 1987 200 mb u-wind, and for (b) DJF 1987/88 200 mb temperature. Difference contours 1 ms^{-1} in (a), and 0.5 K in (b); negative differences dashed. Shading for 90% confidence level.

a) Vertical velocity 500 T63 (6), DJF 1987/88; contours = 25 mPa/s

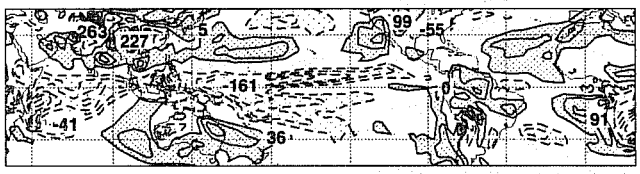

b) Vertical velocity 500 T159 (6), DJF 1987/88; contours = 25 mPa/s

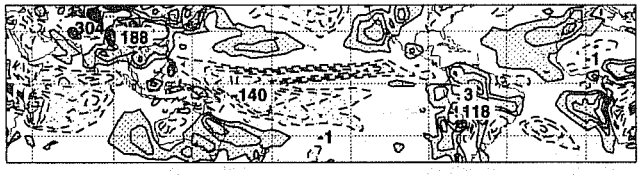

c) Vertical velocity 500 T319 (6), DJF 1987/88; contours = 25 mPa/s

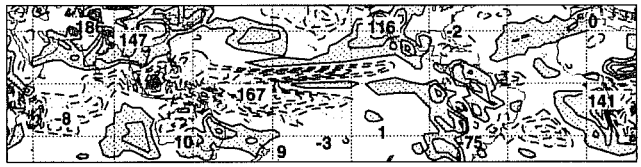

d) Vertical velocity 500 T63 (6), JJA 1987; contours = 25 mPa/s

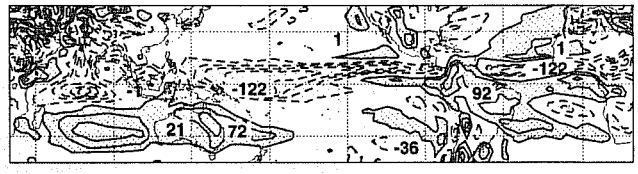

e) Vertical velocity 500 T159 (6), JJA 1987; contours = 25 mPa/s

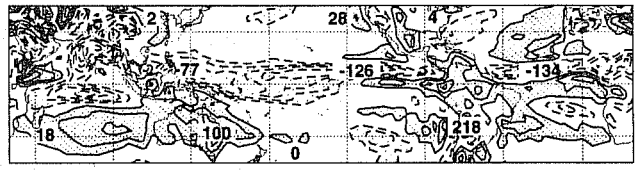

f) Vertical velocity 500 T319 (6), JJA 1987; contours = 25 mPa/s

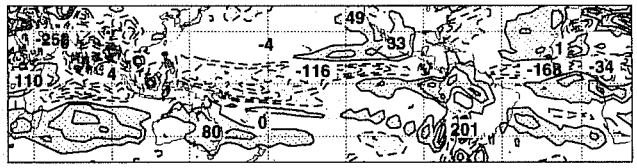

Fig.10 Tropical 500 mb vertical velocity in DJF 1987/88 (left) and JJA 1987 (right) for T63 (top), T_L159 (middle) and T_L319 (bottom). Contours every 25 $mPas^{-1}$. Rising motion coarse stipple (dashed), sinking motion dense stipple (solid).

a) Velocity potential 200 T63 (6), JJA 1987; cont = 2

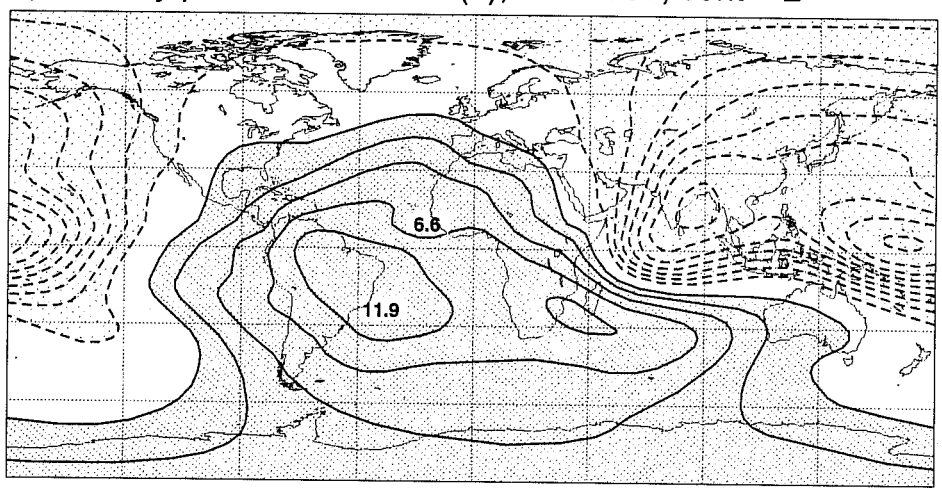

b) Velocity potential 200 T159-T63 (6), JJA 1987; cont = 1

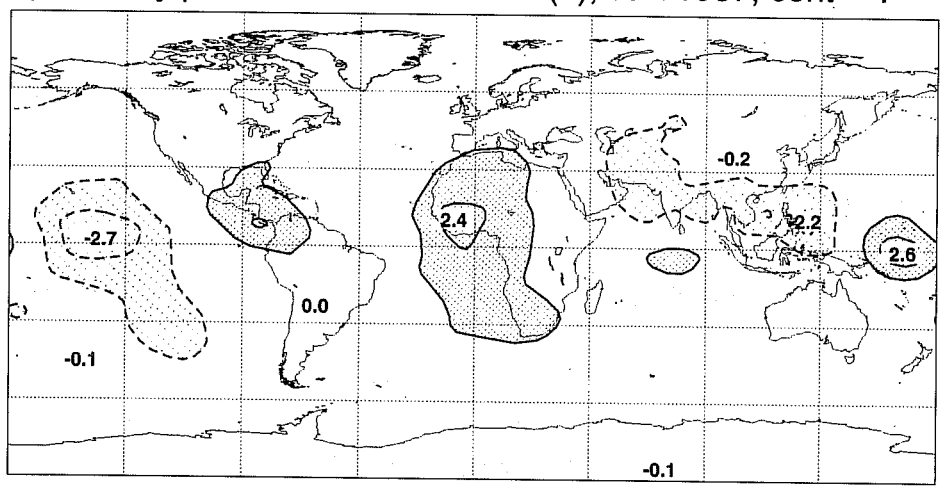

c) Velocity potential 200 T319-T63 (6), JJA 1987; cont = 1

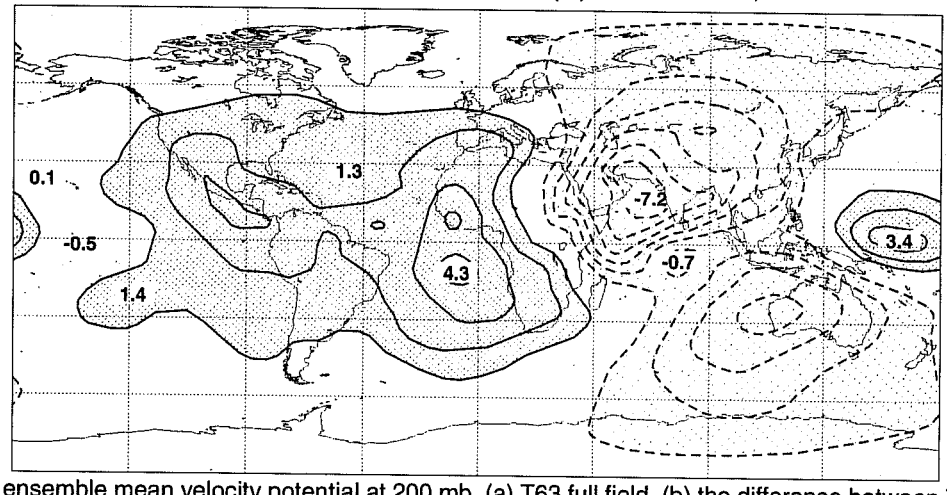

Fig.11 JJA 1987 ensemble mean velocity potential at 200 mb. (a) T63 full field, (b) the difference between T_L159 and T63, and (c) the difference between T_L319 and T63. Contours every 2 x 10^6 m^2s^{-1} in (a) and 1 x 10^6 m^2s^{-1} in (b) and (c).

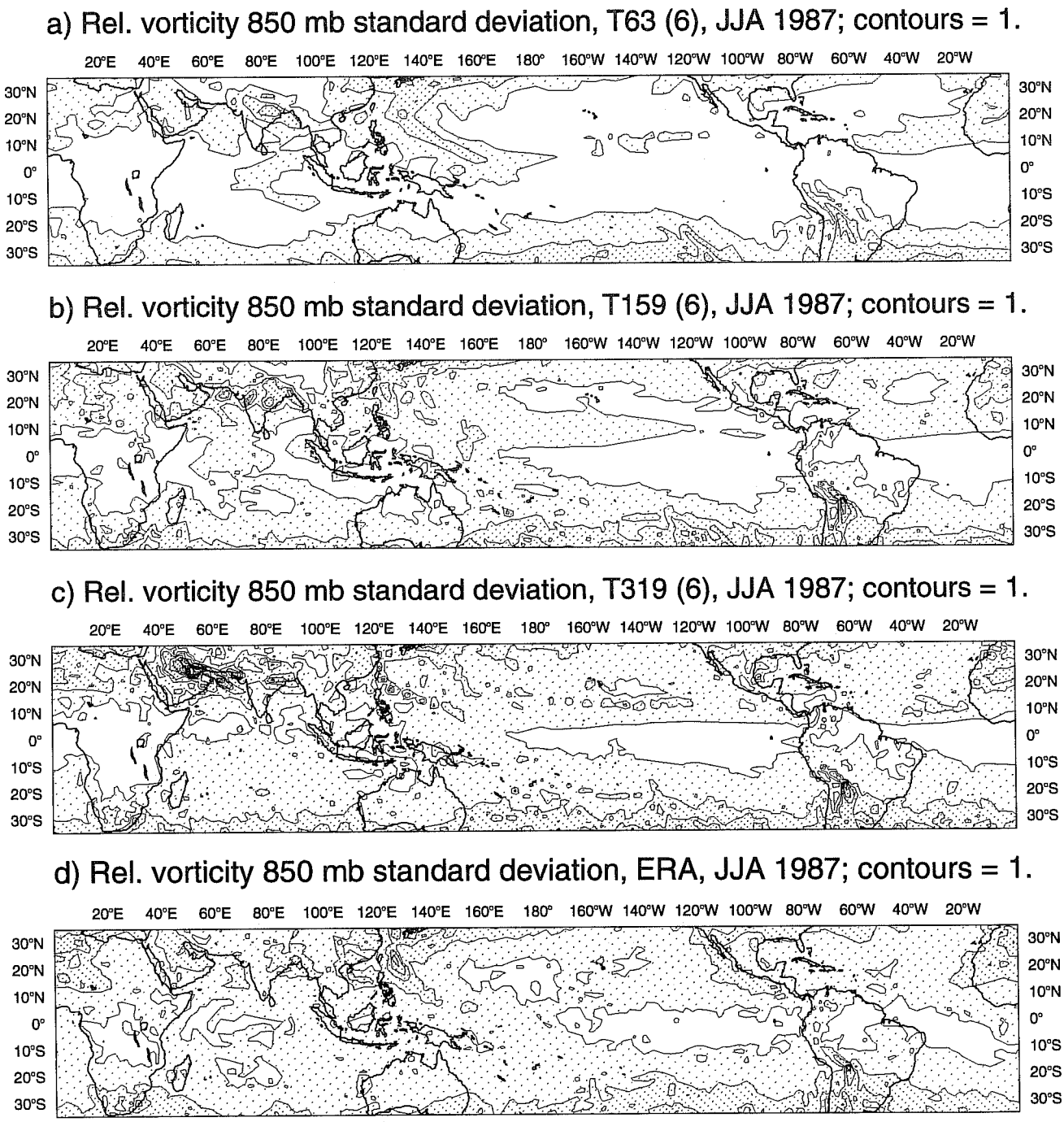

Fig.12 Standard deviation of the JJA 850 mb relative vorticity for (a) T63, (b) T_L159, (c) T_L319 and (d) ERA-15. Contours every 1 x 10^6 s^{-1}.

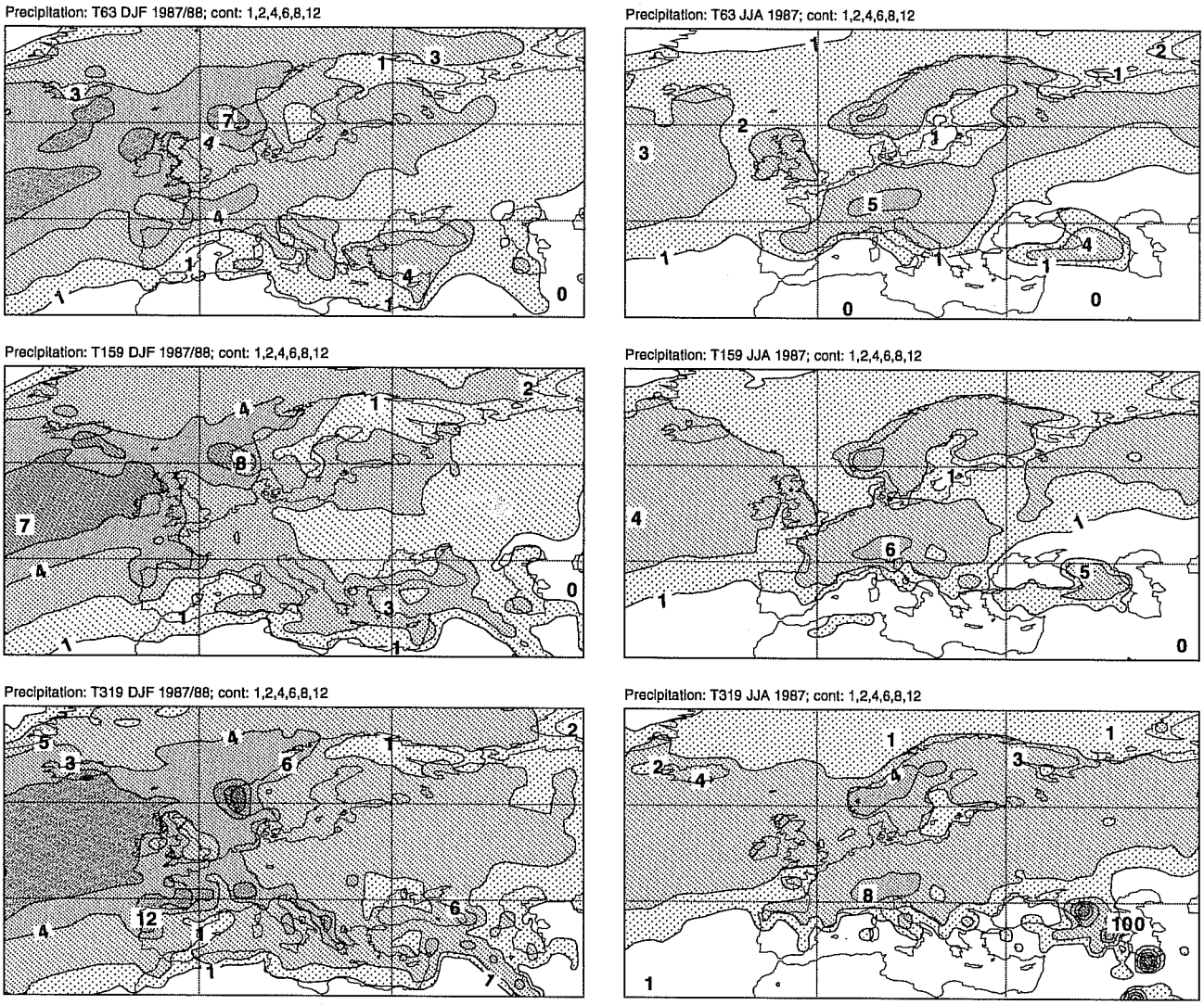

Fig.13 European total precipitation in DJF 1987/88 (left) and JJA 1987 (right) for T63 (top), T_L159 (middle) and T_L319 (bottom) resolutions. Contours 1, 2, 4, 6, 8, 12 mmday^{-1}.

Precipitation: T63 JJA 1987; cont: 1,2,5,10,20,50

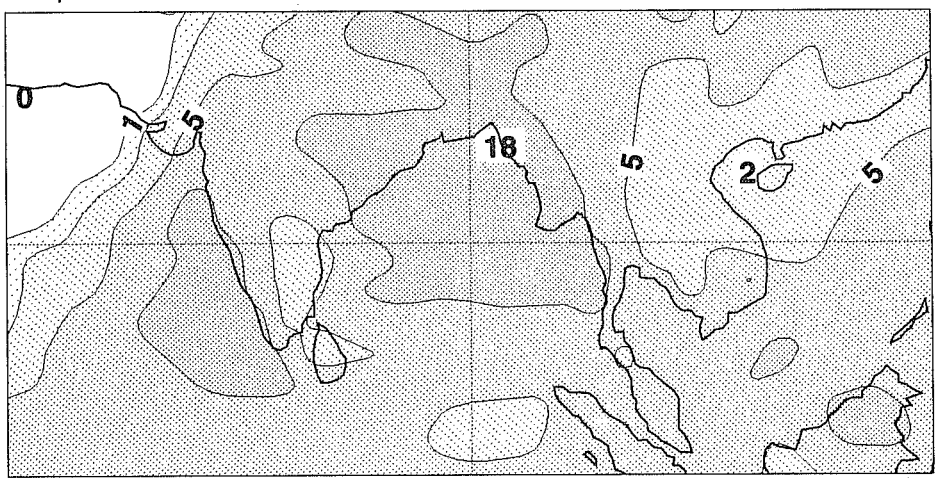

Precipitation: T159 JJA 1987; cont: 1,2,5,10,20,50

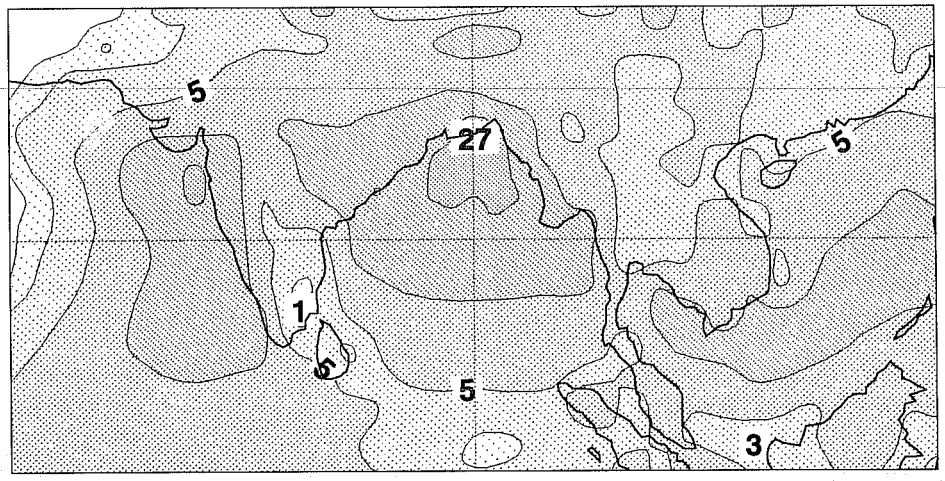

Precipitation: T319 JJA 1987; cont: 1,2,5,10,20,50

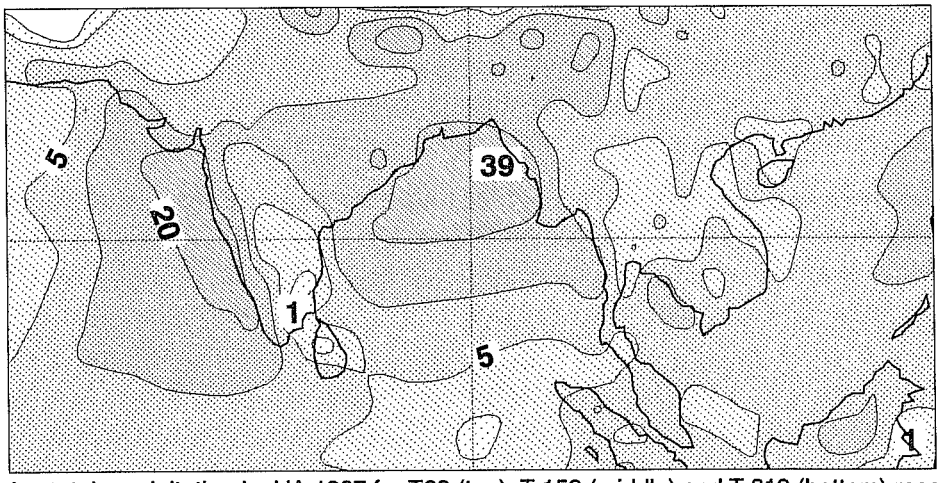

Fig.14 South Asian total precipitation in JJA 1987 for T63 (top), T_L159 (middle) and T_L319 (bottom) resolutions. Contours: 1, 2, 5, 10, 20, 50 $mmday^{-1}$.

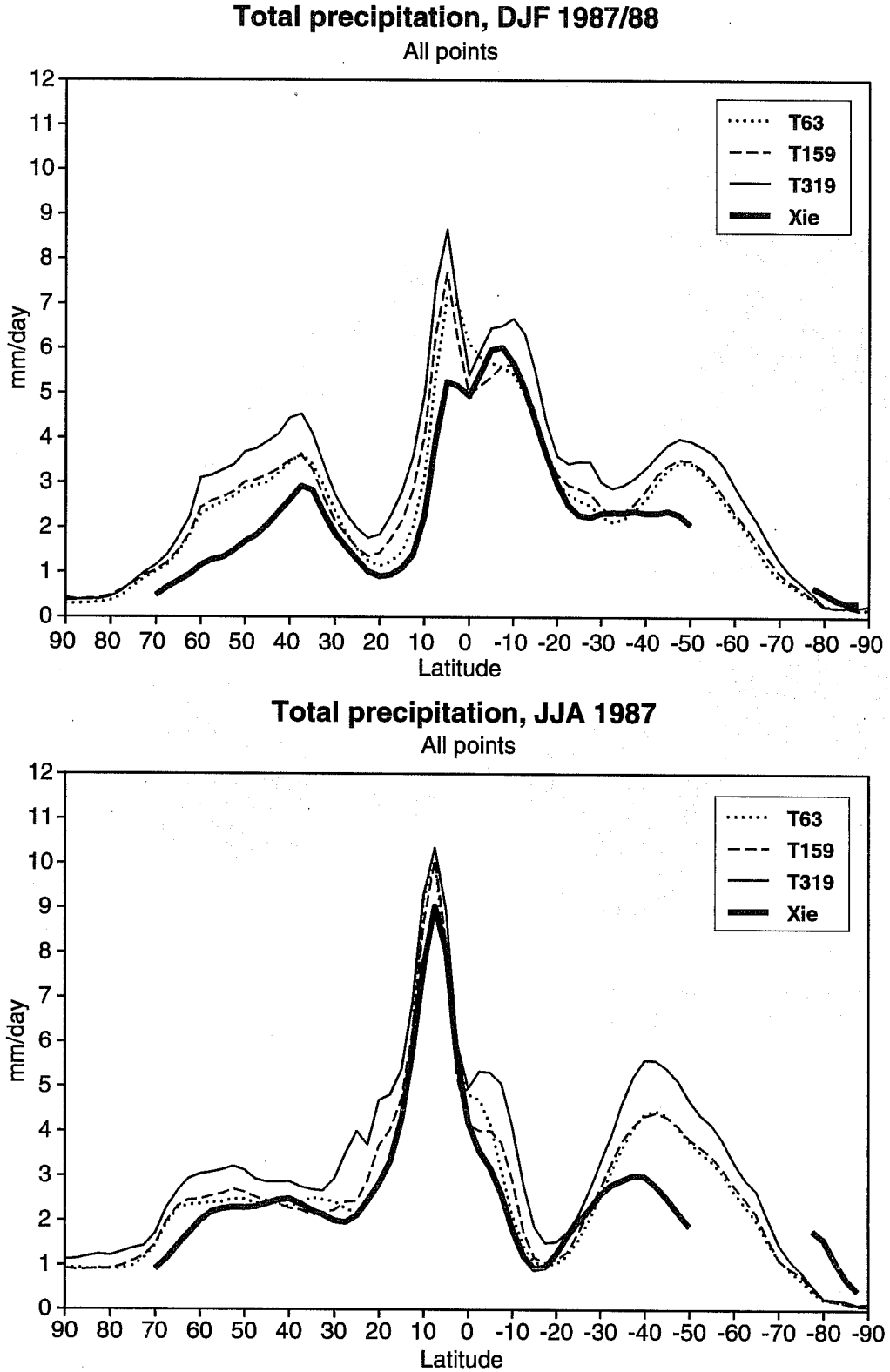

Fig.15 Zonally averaged total precipitation in mmday^{-1} for DJF 1987/88 (top) and JJA 1987 (bottom). Xie and Arkin data thick solid, T63 dotted, T_L159 dashed and T_L319 thin solid line.

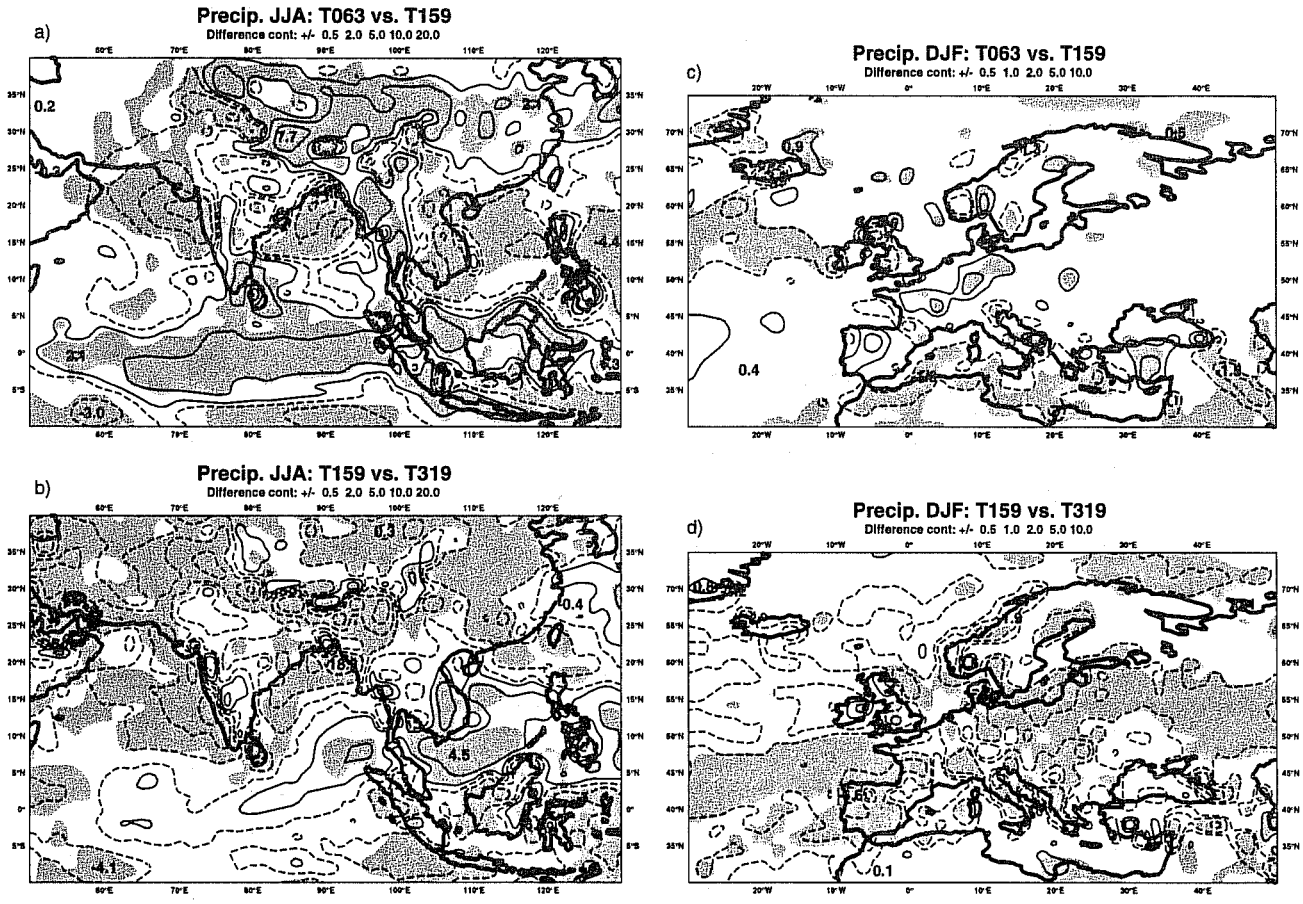

Fig.16 As Fig.8 but for JJA 1987 south Asian precipitation for the comparison (a) T63 minus T_L159, and (b) T_L159 minus T_L319; for DJF 1987/88 European precipitation for the comparison (c) T63 minus T_L159, and (d) T_L159 minus T_L319. Difference contours ± 0.5, 2, 5, 10 and 20 mmday^{-1} in (a) and (b), and ± 0.5, 1, 2, 5 and 10 mmday^{-1} in (c) and (d); negative differences dashed. Shading for 90% confidence level.

Wind stress: T63 DJF 1987/88; Arrow unit 200 mPa; cont: 50,100,150,200,300,400

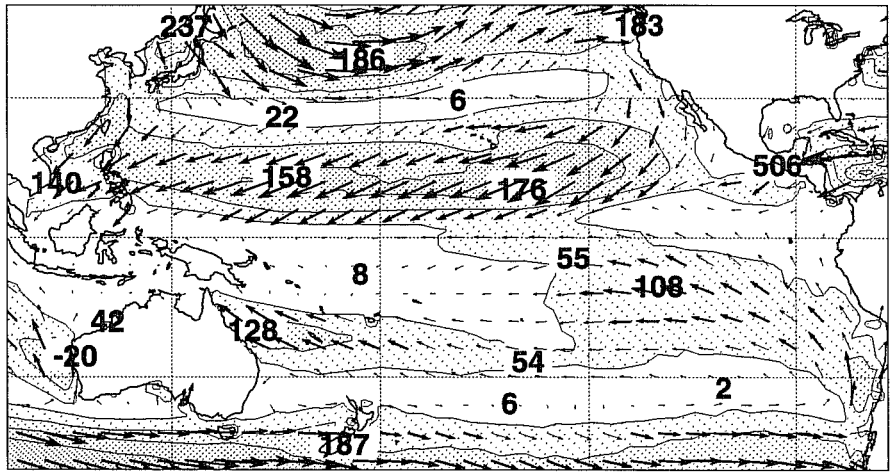

Wind stress: T159 DJF 1987/88; Arrow unit 200 mPa; cont: 50,100,150,200,300,400

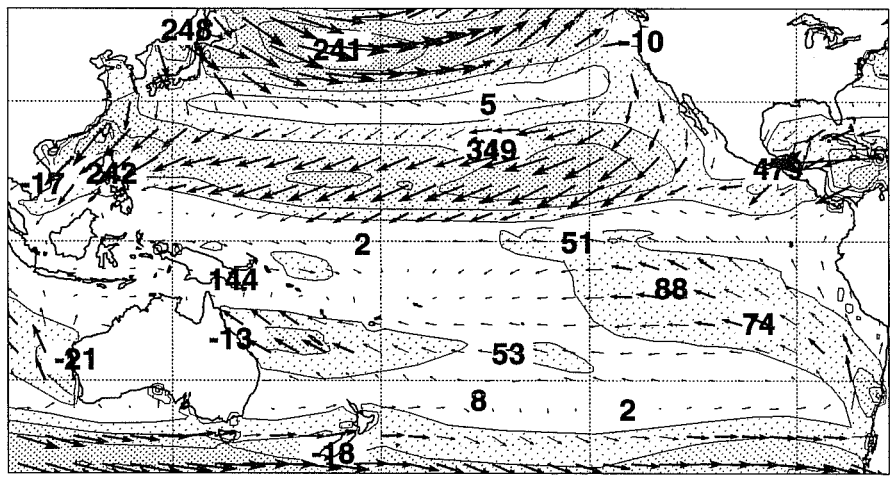

Wind stress: T319 DJF 1987/88; Arrow unit 200 mPa; cont: 50,100,150,200,300,400

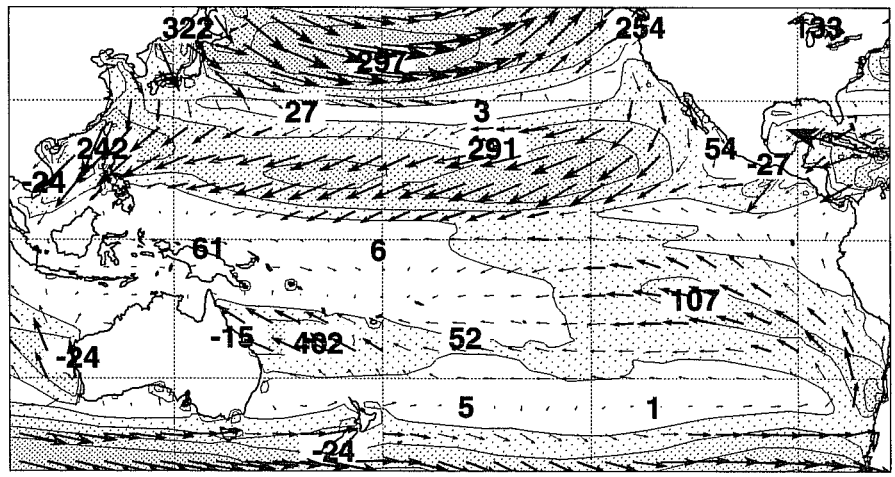

Fig.17 DJF 1987/88 Pacific surface wind stress in mPas for T63 (top), T_L159 (middle) and T_L319 (bottom) resolutions. Contours at 50, 100, 150, 200, 300, 400 mPas.